Possible heat production in some Ni-H and Ni-D systems, revised

Evstigneev N.M.[1,2*], **Ikonnikov A.V.**[2], **Makeev S.V.**[2], **Ryabkov O.I.**[1,2,3], **Skliznev V.V.**[2]

E-mail: * evstigneevnm@yandex.ru
[1] Federal Research Center "Computer Science and Control" of the Russian Academy of Sciences, pr. 60-letiya Oktyabrya, Bldg 9, Moscow, 117312, Russia
[2] LLC 'New Inflow', till 03. Dec. 2019, Leninsky Prospect, 96, Moscow, 119415, Russia
[3] Joint Institute for High Temperatures of the Russian Academy of Sciences, Izhorskaya 13 Bldg 2, Moscow, 125412, Russia

Abstract. The paper concludes two year research on the topic of the possible heat production in nickel-hydrogen (Ni-H) and nickel-deuterium (Ni-D) systems during heating that was initially announced by S.Focardi, R.Habel, F.Piantelli and later reported by A.Rossi and A.G.Parkhomov. The authors developed a new methodology and new testing units that could provide consistent results for the physical community due to high importance of such reports in the wake of energy crisis. The testing units were engineered with such a design that both nonlinear heat losses (convection and radiation) during the experiment were minimized. The experimental methodology is based on the statistical hypothesis testing of the normal distribution from experimental heater power consumption data samples while the temperature is stabilized by the PID controller according to the provided experimental program. This methodology was tested by artificially supplied heat sources and sufficient accuracy was confirmed around 1.5-3.0%. Around 50 experiments with fuel were conducted with various additional ingredients, different forms of Ni, pure hydrogen and hydrogen-deuterium mixtures according to the experiments cited above. No statistically significant levels of the heat production were found in any of the experiments, with less than 1.5% accuracy in terms of heater power consumption.

Keywords: Statistical analysis, Heat production in Ni-H systems, Cold Fusion experiment protocol, Design of experimental protocols

Acknowledgments

This work was financed by the LLC "New Inflow" company until the end of November 2019.

The authors wish to express their hearty thanks to the anonymous referees. Their most useful comments and constructive suggestions helped to improve the paper quality significantly.

1. Introduction and problem formulation

1.1. Current state review

This work is an experimental attempt to verify one of the cold fusion experiments. Under cold fusion in this paper we shall unite all possible abbreviates used, such as Low Energy Nuclear Reactions (LENR), Lattice Assisted Nuclear Reactions (LANR) etc. This publication was inspired by the work of Berlinguette et al. [1] where multiple cold fusion experiments were verified with the highest standards of scientific rigor. However, the paper [1] was short on details. In reverse, we wish to make this paper as detailed as possible. Authors understand the general negative attitude towards such publications but we belive that justified experimental research is needed in order to verify cold fusion in the face of the world energy crisis. Example of such positive approach in this field is the work of McKubre's team at SRI [2] or the work of Peter L. Hagelstein [3]. Such work is necessary in order to guide the scientific community in the right direction and filter out wrong (and sometimes scam) results. This paper doesn't review the full list of cold fusion theories and experiments (started back in 1989 by M.Fleischmann and S.Pons [4]) and only focuses on the subject, namely, energy production in nickel-hydrogen (Ni-H) and nickel-deuterium (Ni-D) systems, where hydrogen (deuterium) is used in gaseous forms and Ni is used in either powdered or bulk forms. Early reports of heat production in Ni-H and Ni-D electrochemical cells, first noticed in [5], are excluded from our review. An interested reader can be referred to the papers [6, 7, 2, 1] for detailed general reviews from different points of view at different temporal slices.

The first report of the anomalous heat production in bulk Nickel loaded with Hydrogen (Ni-H systems) was published in 1994 by Focardi, Habel and Piantelli [8] where the evidences of excess heat production with the power of 50W from the hydrogen/deuterium loaded nickel rod are reported. The vacuum chamber was made of stainless steel. The chamber could be pumped out to vacuum or supplied with hydrogen/deuterium. A platinum heater powered by DC voltage stabilized power supply and a metal rod were placed inside the chamber. The metal rods used were made either of Ni or stainless steel. The latter was used to obtain data when no Ni was loaded and, hence, no heat production effect could be expected (control experiments). A technical vacuum was achieved at first. When the temperature was $400^{\circ}C$, the hydrogen was injected into the chamber with pressure from a couple of torrs up to 1 bar. It was found that the maximum "filling" of the nickel sample occurred at temperature above $173^{\circ}C$ and gas pressure below atmosphere (around 0.051 bar). Later the temperature was increased up to 400–$450^{\circ}C$ (heater power around 150W) and anomalous heat production of around 20-50W was reported by comparing the temperature of control experiments made of

stainless steel rod vs. experiments with Ni rod. Nuclear nature of the phenomenon is assumed by measuring γ–radiation and neutron emission from these experiments [9, 10]. In general, more information on the experiments that were conducted in this field by Italian scientists can be found in the report [11].

Further research in this field was continued by the Italian group formed by authors of the paper [8] and A.Rossi. Results of their hydrogen device are presented in the reports by Levi et al. [12, 13] where independent testers performed energy measurements. This report gives details on, so called, E-CAT device that was promoted by A.Rossi as a commercial product, thus the device is proprietary and no technical details about the device are publically available. Interesting to note that the patent application on this device [14] contains no information about the nuclear nature of the excess heat, except only stating it. The report is based on thermal analysis of the devices containing (possibly) Ni-H system at temperatures from $700^{\circ}C$ up to $1200^{\circ}C$. Some detailed information is contained in the report regarding energy estimate. Estimation of energy by the emission of thermal radiation through the infrared camera thermography measurements was used as the main tool of the experiment, convectional and diffusive losses were considered negligible.

Some critical papers were published [15, 16] after the reports had been released, we refer readers to these reports for more details. The main drawbacks of the experiment, according to the reports, were related to the incorrect measurements of thermal radiation by the assumption of the gray-body radiation from the alumina surface of the reactor. This issue is addressed in [15]. Other issues are related to the authors of the reports [12, 13] (some authors worked with A.Rossi before and cannot be considered independent), extraordinary ^{62}Ni isotope shifts, absence of the model that can be used to estimate the shape of the thermal distribution on the surface etc. As the result, the conclusions of the report [12] are undermined.

Another research group related to the Ni-H experiments that reports positive results is led by A.G.Parkhomov. The group started to replicate the E-CAT device by A.Rossi using his patent application with reports of success in late 2014. Then the group continued the experimental work making different variations of Ni-H reactors. Most publications are in Russian, the following English paper [17] contains a review of the group's results and can be cited here. The reactors are mostly made of ceramic tubes covered by concrete or other insulating material. The Ni in powder forms is used as a fuel. Lithium aluminium hydride ($LiAlH_4$ or LAH for short abbreviation) is used (as was stated in the A.Rossi's patent application [14]) in some reactors as an additional fuel component. Hydrogen was supplied by either an external source or by the thermal decomposition of LAH during heating. The Ni powder was extensively pretreated with hydrogen at temperatures around $300^{\circ}C$—$400^{\circ}C$ (periodic vacuumization and hydrogen treatment during a couple of days) in order for the excess heat to take place afterwards during further heating. A pressure gauge was also used to estimate the hydrogen pressure in the reactor. Decrease of pressure was detected in all experiments after this treating, even with the pressure level below atmospheric level. Authors assumed that the hydrogen was consumed by the Ni powder. The heater temperature was controlled by the automatic PID controller. The energy was estimated using both control experiments comparisons and flow through calorimetry. The latter was calibrated by the

product lost coefficient with the short time control experiment, see section 7 in [17] for details. Long term experiments (up to half a year) were conducted, reporting excess heat production in all tested reactors. A coefficient of performance is reported around 1.2 — 1.77 and up to 3.0 for higher temperatures up to $1290^{\circ}C$ and later up to $1500^{\circ}C$ (in a Russian publication). Isotope analysis was also conducted using inductively coupled plasma mass spectrometry with no significant changes in the isotopic composition of Ni, except by the report of the Uppsala university. However, A.G.Parkhomov believes (personal communication) that the result was misinterpreted. Multiple occurrence of chemical elements of natural isotope composition is registered [17] by the use of electron scanning microscope and laser-induced breakdown spectroscopy. Authors also suggest different theoretical exotic nuclear reaction mechanisms such as fission of tungsten or the nickel hydrogen nuclear reaction.

This research was also partly inspired by the results of the Parkhomov's group. The bonus for this group research is that it is transparent and publicly open. The experimental approach seemed correct and scientifically solid. Authors had personal communication with A.G.Parkhomov on the materials used and on the fuel pretreatment protocol. However, some things should be investigated deeper, in our opinion. First, duration of all control experiments was much less than experiments with loaded fuel, so one questions if the stationary regime took place in control experiments (regarding degradation of construction materials, permeability of liquid and gaseous components of fuel and construction elements at high temperatures, surface oxidation and so on). The design of the test units was far from perfect (as can be seen in pictures in the publications) and control experiments were newly made reactors (the sizes and physical properties of these reactors could vary), so the uncertainty interval can be extended because of this. Second, some experimental reactors had no deflection of thermal radiation and convection as can also be seen from the provided pictures, so strong nonlinear effects could take place. Third, the calorimetry was self-made and no conditions were guaranteed to insure isoperibol calorimetry. In such conditions, in our opinion, the short term calibration experiment can't be applied to the long term experiment with active fuel due to the possible non-stationary change of the heat flux through jackets of the calorimeter which is caused by the changes of the construction. Finally, the drop of pressure below atmospheric level at temperatures around $300^{\circ}C$—$400^{\circ}C$ could take place because of the hydrogen permeation through heated metal parts of the construction. In this case, a partial hydrogen pressure must be considered, which is almost absolute zero in the surrounding atmosphere [18]. All these facts call for deeper investigation.

Several experiments with Pd-H or Ni-H systems were performed by T. Mizuno et al. [19, 20]. These experiments contain multiple data with analysis of input and output power consumption, chemical element analysis and other experimental details.

It is always desirable to validate experimental data vs theoretical results available in literature. Unfortunately, no satisfactory theory exists to quantitatively predict cold fusion experiments neither in nuclear nor in weak coupling sense. Authors are aware of different theoretical attempts to describe excess heat production in Ni-H and Ni-D systems. However, there is only one theory by P.L.Hagelstein [21, 22] that can give qualitative description of the assumed phenomenon. Hence, no theories are verified in this research.

Authors of this paper are not new to this field having worked alongside cold fusion for almost 10 years (as a part-time job), see [23, 24, 25], where we helped to develop new simulation methods, tested some theories (simulation of ultra cold neutron fluxes on targets and prediction of the isotope shifts in materials, test some ideas on the Widom-Larsen theory, reported in ICCF-19) and helped to automate experiments and obtain more precise experimental data. We also had multiple contacts in the Russian Cold Fusion community (including A.G.Parkhomov and A.I.Klimov). Having that much experience dealing with experimental work in the Cold Fusion, we realized that experiments in this field require more rigorous approach, especially because of the skepticism of the scientific community. This paper covers our experimental work in an attempt to do so.

1.2. Problem formulation and our approach

The Coefficient Of Performance (COP) in most papers is measured as:

$$COP = \frac{E^T_{out}}{E^E_{in}}, \tag{1}$$

the ratio of the output thermal energy (E^T_{out}) to the input electrical energy (E^E_{in}) in one way or another (for example, many authors are using the ratio of input and output power instead of energy. In this case, the energies in (1) are interpreted as energies averaged over a short period of time). Usually, E^E_{in} is measured directly, but E^T_{out} can be measured, generally, in two ways: direct methods via the use of calorimetry or thermal radiation; comparative methods when additional control experiments are used to form a baseline.

Not willing to drop the shadow of doubt on the scientific honor of all cited scientists in the previous subsection, we stress that the deviations in (1) can be caused not only by anomalous heat production, but by tricky effects in measurements, heat dissipation mechanisms and construction degradation.

For example, some non-stationary temperature dependent process of change in the fraction (1) can mimic the effect of anomalous heat production. First, an abrupt change in hydrogen natural convection with outside reservoir or its blockage due to anisotropic shifts in the device construction at high temperatures can cause such effect. Relatively simple estimate shows that the change in convection can ”produce” around 30-80W of heat due to the high values of heat capacity and heat conductivity of hydrogen in the above cited devices. Second, the change of the emissivity on the outer surface of the container material. Most experiments are conducted at high temperatures ($800^\circ C$–$1200^\circ C$) where thermal radiation becomes a dominant energy dissipator ($\sim T^4$). If the experiment is exposed to oxidation and emits thermal radiation freely (as can be seen in [20, 17] and other experiments) then even the slightest change of emissivity can ”generate” heat power compared to the control experiment. Incorrect calibration (for example incorrect thermal radiation account in [12, 13]) can ”generate” excess heat even in direct measurements of E^T_{out}. Such mechanism of possible faulty excess heat is well demonstrated in the comments to the A.Rossi’s report by T.Clarke [15].

Next, the degradation of a heating device can cause decrease of input electrical power compared to the control experiment (in the estimation of E_{in}^{E}). This can be rolled out if the resistance of heaters was measured at the beginning and ending of each experiment, or by using a digital power meter with high discretization. However, cited papers usually lack such details, thus giving food for doubts. Finally, partial melting of the reactor material with further solidification can change heat conduction as well as both convection and radiation inside the testing units with obvious false decrease of input energy or increase of measured temperature on the reactor measuring point.

The authors worked in the LLC "New Inflow" company at the time of experimental planing, where the investor was focused on the energy output measurements. Hence, the problem was formulated in terms of energy production monitoring. The main goal for authors was to perform a rigorous, statistically justified and relatively simple procedure to verify the excess heat production in Ni-H and Ni-D systems. The plan of experiment was based on different sources: papers by [8, 17], personal communications with the Russian Cold Fusion community, including A.G.Parkhomov and personal ideas, based on some modifications of the Widom-Larsen theory.

In the wake of the previous section, we believe that the following principles must be implemented in any experiment dealing with cold fusion.

The Principles

- *Minimize all possible false positive (FP) effects listed above.*
- *False negative (FN) results are less important than false positive (FP) results.*
- *Perform statistical analysis and obtain measurement uncertainty.*
- *Decrease uncertainty as much as possible to increase sensitivity.*
- *Design experimental units in such a way that they can withstand long treatment of high temperatures and multiple loading of materials with minimum changes in the construction.*
- *Minimum or no human interference in the experiments is necessary.*
- *Dummy experiments have the same duration and must be performed on the same experimental units as fuel loaded experiments with the same conditions.*

The general idea of the experiments is the following. The heating process, gas and vacuum line supply valves and measuring are handled by the computer program by providing the set temperature, gas and vacuum supply programs and collecting results. Such approach is perfectly repeatable. The control of the temperature is performed using the tuned high precision PID regulator. Experiments with no fuel (a-priori known fact that no heat production can take place) provide a statistical baseline for the heater power consumption from the grid. Generation of additional energy in thermal form in reactors with loaded fuel would result in the increase of the observing temperature due to good thermal insulation of experimental units. This leads to the drop of heater power to such level that the controlled temperature deviation from the set temperature is minimized by the PID controller. As the result, heater energy consumption from the grid should drop and be lower for experiments with

heat production compared to the statistical baseline. This should be noticed as a drop of graphical representation of power consumption below such levels that this drop is considered statistically significant. The calibration on experimental units must be carried out to confirm the statistical significance levels.

The paper is laid out as follows. The next section describes the experimental methodology, the uncertainty measurement method and the design of experimental units that were used. This section also includes experimental programs that were developed to cover fuel treatment with hydrogen and vacuum, as well as long experimental runs on different temperature levels. Then the experimental results are presented, including statistical hypothesis testing results and estimation of sensitivity. Next, the experiments with loaded fuels are described. The paper is finalized by the Discussion section, where we speculate on the origin of the negative results. One false positive (FP) experiment that was obtained at the early stage of the methodology tuning is discussed. This discussion gives more information on the nature of possible FP results of other authors and highlights bonuses of the final suggested methodology.

We understand it may seem odd that so much information and details are presented describing an experiment with a negative result. An analogous paper in the traditional filed of applied physics would consist of a couple of pages. But we insist on detailed description of the work because the field of cold fusion is still not widely accepted and one needs as much information as possible in order to replicate, test and draw conclusions based on this information. We present a very thorough description of our methodology, experimental protocols and statistical testings in order to allow any interested groups to repeat these experiments. If one is not interested in full details, one can skip to the Section 3.2, where the resulting experimental data is presented.

2. Methodology, uncertainty measurements and experimental units design

2.1. Experimental methodology, uncertainty measurements

In the general methodology, experimental units are considered as black boxes. The black box contains an electrical heater that is supplied by the external electrical power source and the set of observation points where the temperature and pressure is monitored. It was chosen to use supplied electrical power as the controlled and indicative parameter, where the temperature at fixed points in the black box was used as the observation parameter. Pressure points are used only for monitoring. It is also assumed that the characteristic time of the process of interest is slow in terms of measurements, i.e. discretization time is bounded from below by 1 second and from above by 5 seconds. Each black box can have two states - empty and loaded. Empty state is when the fuel (any possible combination of Ni and other ingredients) is not loaded, thus no excess heat is expected. The loaded state is when the fuel is loaded and excess heat may be expected.

The overall number of different experiments on a single black box construction B is defined as S. Experiments are conducted by the set of fixed programs $\Pi = \{\Pi_j\}$. Each

program contains the desired variance of the observation parameter in time (relative to the experiment starting point), i.e. $\forall j = 1...S; T^{j,set} \in \Pi_j$ and $T^{j,set} = T^{j,set}(t)$ defined at any continuous time t. Also, each program Π_j may contain additional necessary properties for the execution of the experiment. The program is controlled by the computer and is enforced through the software proportional-integral-derivative (PID) controller by the analysis of the temperature $T(t_q)$ and adjustment of the appropriate electrical power on the heater $N^j(t_q)$ by some hardware identified later. The temporal variable t_q is a discrete variable defined by the whole controlling system sampling discretization with time steps $\tau_q = t_{q+1} - t_q$, $1 \leq \tau_q \leq 5$ s., for $q > 0$. The function $f(t)$ can be restricted to $f(t_q)$ in the natural way. The inverse recovery of the continuous function $f(t)$ from the discrete $f(t_q)$ is performed by the monotone spline interpolation. The PID controller with vector of coefficients $\mathbf{k}$ insures, that:

$$e_j(t_q) := \left\| T^{j,set}(t_q) - T(t_q) \right\| \to \min_{\mathbf{k}}. \tag{2}$$

The coefficients are obtained by the process of the PID tuning for each black box construction B and are fixed for each construction. The appropriate electric power $N_l^j(t_q)$ is obtained for the l-th execution of the program Π_j for the fixed black box construction B, i.e. for each experimental unit. One can define the number of total executions of Π_j. This number is denoted as K_j^e for empty black boxes and K_j^f for loaded. All experiments with empty black boxes are called 'statistical' and all experiments with loaded black boxes are called 'credible'. The sets N^j (for statistical experiments) and Ng^j (for credible experiments) contain all pointwise electrical power data for all total number of executions for the program Π_j. The set of all possible fuel mixtures is defined as F_B^j for each program and black box construction. In order to perform statistical analysis, some axillary functions μ, σ and $\mathscr{F}$ over discrete data are introduced. This analysis can be performed on the data that is divided into intervals, designated as $\{[q_1^r, q_2^r]\}_{r=1}^R$. The union of these intervals does not necessarily cover the whole time of execution. Their precise definition is given below and has no influence on the general methodology.

The experimental methodology itself is defined as an abstract Algorithm and filtering functions that are applied in this algorithm with statistical hypothesis testing. The details on the Algorithm are provided in the Appendix A. One can notice that the Algorithm has no dependence on a particular black box construction or a particular program. Thus, this algorithm can be viewed as a stand along procedure to verify any experimental claim of excess heat production for arbitrary program and black box units construction. The sensitivity of the whole methodology is determined by the particular choice of the program and construction of units, as well as by other hardware related issues. For example, this methodology will always give negative results for poorly constructed test units and faulty hardware by increasing the variance during the statistical analysis over the obtained population data. Thus, false positive results are minimized or even removed.

This complies with the provided above principles in subsection 1.2 for any experiment dealing with cold fusion. One can rebuke us with extreme skepticism in using maximum functional for σ, see Appendix A. This note is ruled out by the calibration experiments, see Section 3. The analysis of data, including normality and $p\sigma$ tests, are performed by using

python 3.7 with *pandas*, *numpy*, *scipy*, *statsmodels*, *sklearn*, *pylab* and *matplotlib* modules.

2.2. Design of schematics hardware and experimental units

This subsection describes a particular design of both hardware and experimental units that are used in the Algorithm 1. The hardware contains power electrical lines and controlling devices, shielded measurement lines and devices, gas lines (hydrogen, deuterium and argon) and vacuum lines, connected to the rotary vane vacuum pump D.V.P. DB.2D with the residual pressure of 0.005 mbar. All lines are equipped with electrically controlled valves, including both operational and emergency. This approach minimizes the human influence during the experiments to almost non-existent level. Again, this complies with the provided above principles in subsection 1.2.

The details about the controlling and measuring hardware are provided in the Appendix B. The main target of all experiments is located in the experimental units, designated "1" in figure B1. Its particular designs are discussed below. The main requirements for these units are to withstand high temperatures, have minimal degradation from experiment to experiment, measurements points are fixed and are not changed from one experiment to the other (according to the principles in subsection 1.2).

All experimental units contain the main electric heater, vacuum pressure gauges, temperature gauges and one or several reloadable capsules that either contain control material or fuel. These capsules are called reactors for short, so one uses fuel reactors for credible experiments and control reactors for statistical experiments. Two main experimental units were engineered.

The first experimental unit is aimed at the experiments with sealed reactors where fuel and hydrogen/deuterium are stored in a confinement and the outer side is subject to inert atmosphere. The hydrogen pressure up to 200 bars can be achieved in these small reactors during thermal decomposition of the LAH. More details are provided in Appendix C.

The drawing of the assembly of the whole unit is presented in figure C1. The schematic of the sealed reactors used in this experimental unit are shown in figure C3. An example picture of the sealed and loaded reactors is provided in the Appendix J. The process of the fuel loading is described in the section below. The experimental program for these reactors is designed in such a way that the hydrogen remains in reactors at least for $T^{1,set} \leq 1000°C$. The maximum hydrogen pressure in credible experiments is around 200 bars at $400°C$ in Nickel containers.

The second experimental unit is aimed at the experiments with open reactors for higher temperatures where fuel remains in hydrogen/deuterium atmosphere over the whole time of the experiment. The hydrogen pressure is around 1.05 bar, slightly greater than the atmospheric pressure. The process of the fuel preparation can be executed in the unit itself, allowing one to obtain more control over the fuel pretreatment and pressure monitoring.

The schematic of the unit section is presented in figure D1. The design of the open reactor is given in figure D2. The picture of the unit and some internal parts are available in the Appendix J. The experimental unit is designed to be operational in either hydrogen/deuterium

or in vacuum. No other gas is allowed. This construction allows one to change the reactor to the one used in the first experimental unit (scaled to size) by small changes in the construction. The sizes of the radiation, convectional and thermal insulations ensure that almost all possible nonlinear effects are blocked and linear diffusive thermal dissipation process is dominated during heating.

2.3. Notes on the uncertainty

All random errors are included into statistical experiments and are taken into account by the suggested methodology. These errors include measurement errors, assembly errors in experimental units, random electrical noises, random errors due to human interaction with experimental units during loading and unloading of the reactors etc. For this reason, each statistical experiment is conducted at a full scale, including cooling, opening and reloading of the experimental unit with shuffled control reactors. So each statistical experiment is performed identically to the credible one.

The systematic errors are not important since the methodology is based on the comparative method to identify excess heat production in full vs. control reactors, as long as the measuring units with this systematic error are not replaced by other measuring units with other systematic errors. For this reason, three digital power meters were calibrated and could be replaced in case of emergency with relative error less than 0.1% in voltage ranges $210-240V$ and current ranges $0.2-3$A. A special heating device was constructed that allowed one to calibrate and tune all thermocouples in the wide range of temperatures up to $1300^{\circ}C$ in the inert atmosphere or in the hydrogen. The change of some thermocouples and appropriate modification of voltage-signal curves in ACDs resulted in negligible effect on the systematic error in the levels of heater power set by the PID controller.

2.4. Experimental programs

The description of particular programs (elements in the set Π) are presented in this subsection. All experimental programs were adjusted in such a way that those would cover the experiments of other authors as well as test our ideas.

- For the first experimental unit, a single experimental program is used. The program consists of defined temperature T^{set} values and inert gas pressure values inside the dome, both as functions of time. The same program is used for both, statistical and credible experiments.

  It is assumed that the unit is cooled down to the laboratory temperature at the beginning. The pressure program is a simple process of initial vacuumization of the dome with later inert gas injection up to the pressure level of 1.1 bar (above atmospheric pressure on 0.1 bar). The temperature program starts as soon as the pressure reaches the set value. Such pressure value is maintained during the whole experiment duration until the internal measured temperature becomes close to the room temperature at the end. So the inert gas is automatically released during heating and injected during cooling.

Table 1. Program $T^{set}(t) \in \Pi_1$ for the first experimental unit. The time is relative to the start of the statistical testing. Time t_1 shows cumulative duration and t_2 shows stage duration.

t, sec	T^{set}, $^\circ C$	t_1, hours	t_2, hours
0	15	0	—
19440	400	5.4	5.4
91440	400	25.4	20
127440	1100	35.4	10
145440	1200	40.4	5
181440	1200	50.4	10
199440	1250	55.4	5
253440	1250	70.4	15
271440	1100	75.4	5
289440	15	80.4	5

The temperature program is defined by the temperature points provided in table 1. The linear interpolation is used between these points. The intervals between neighboring points are called stages. So one can see that there are stages of constant temperature and stages of linearly varying temperature. The duration of each stage is given in the third column in table 1. These durations are selected on purpose such, that all experimental protocols of other authors are satisfied. Namely, the level of $400^\circ C$ is used in [8, 12] to register anomaly heat production and in [17] to prepare the nickel powder by loading hydrogen. The next level of $1100^\circ C$ is used in [12] as the temperature when the first anomaly heat production is registered. The level of $1200^\circ C$ and $1250^\circ C$ is the level of guarantied heat production according to [17]. The temporal duration of all stages is also selected according to the above-mentioned publications. Particular combinations of loaded fuel and its pre-treating are discussed in the next subsection.

- Two separate programs are used for the second experimental unit. The program consists of defined temperature $T^{set}(t)$ values and hydrogen gas pressure values inside the operational chamber, both as functions of time. Programs for statistical and credible experiments are the same in the statistical region ($t \geq 0$ in tables) and different in the initial region ($t < 0$ in tables) since the second experimental unit is designed such that it can be used for both fuel pretreatment and statistical experiment. The pressure program is different depending on the fuels used in the preparation region ($t < 0$ in tables) and is the same for the statistical region ($t \geq 0$ in tables). This allows to shorten the statistical experiments using shorter initial stage. The pressure program for $t \geq 0$ is defied by keeping hydrogen or deuterium pressure a little above the atmospheric pressure (around 1.02 bar) in the operational chamber. So the gas (hydrogen or deuterium) is automatically removed from the chamber during heating and injected during cooling to keep the pressure level.

  The first temperature program for the statistical experiment is presented in table 2. The temperature levels and temporal lengths of stages are selected by the same reasons as

Table 2. Statistical program $T^{set}(t) \in \Pi_2$ for the second experimental unit. The time is relative to the start of the statistical testing. Time t_1 shows cumulative duration and t_2 shows stage duration.

t, sec	T^{set}, $^\circ C$	t_1, hours	t_2, hours
-70250	15	0.0	—
-36000	700	9.5	9.5
0	700	19.5	10.0
20000	1100	25.1	5.6
40000	1200	30.6	5.6
76000	1200	40.6	10.0
96000	1300	46.2	5.6
132000	1300	56.2	10.0
132010	15	56.2	0.0

Table 3. Statistical program $T^{set}(t) \in \Pi_3$ for the second experimental unit. The time is relative to the start of the statistical testing. Time t_1 shows cumulative duration and t_2 shows stage duration.

t, sec	T^{set}, $^\circ C$	t_1, hours	t_2, hours
-149750	15	0.0	
-123000	550	7.4	7.4
-87000	550	17.4	10.0
-79500	700	19.5	2.1
-43500	700	29.5	10.0
-36000	850	31.6	2.1
0	850	41.6	10.0
7500	1000	43.7	2.1
43500	1000	53.7	10.0
51000	1150	55.8	2.1
87000	1150	65.8	10.0
94500	1300	67.8	2.1
130500	1300	77.8	10.0
130510	15	77.9	0.0

previously discussed. The level of $1300^\circ C$ for the temperature is used as the best obtained result in [17]. Only levels of $T > 700^\circ C$ are statistically verified in this program. The assumption is as follows: if the excess heat is observed for lower temperature levels, then it can be observed for higher ones or can be detected in the first experimental unit.

The second temperature program for the statistical experiment is presented in table 3. It contains the same ranges of the set temperature but different duration and number of stages where the temperature is kept constant. This allows one to perform better statistical analysis in the constant temperature regions. However, the statistical region

starts higher at $T > 850°C$.

2.5. Fuels and gases used; fuel pretreatment

All gases used are of high purity. The inert gas in the first experimental unit was the argon with purity of 99.998%. The hydrogen and deuterium gases were obtained using programmable automated electrolysis device (GVCh-36A by the russian company KhimelEktronika) from the distilled light and heavy water, respectively. The device guarantees purity of hydrogen/deuterium up to 99.9999% for purely distilled light/heavy water.

According to the most of the cited sources, the main components of the fuel are the nickel (Ni) and the lithium aluminum hydride ($LiAlH_4$ or LAH) as the optional addition. The LAH produced in China was used with purity of 97% that is available on the market (the same LAH was used in all Parkhomov's experiments, as the only available in the open Russian market). Nickel of different forms (bulk and powdered), dispersities and purities was used and presented in the Appendix E. The mass of Ni powders that were loaded into reactors varied between 0.9 and 4 grams for each loading, and the mass of LAH varied around 0.05-0.2 grams. The provided ratio of Ni/LAH mass loading was dictated by the expected volume of hydrogen release after the chemical dissociation of LAH. The same Appendix E contains different fuel combinations that form the set F_B^j of all fuels in all experiments. Some experiments on the second experimental unit had durations up to a couple of weeks and required periodic vacuumization and injection of different gases. This process was automated in order to perform fully unmanned experiments.

Different fuels, protocols for their treatment and motivation for the fuel selection are listed below:

- Ni0 is the bulk Ni material that was used in the production of the reactor itself. When the temperature rises, the hydrogen inside the sealed reactor begins to permute through the reactor walls (made of bulk Ni) with increased intensity. This will result in the maximum possible Ni saturation with hydrogen (if any). The hydrogen pressure in the first experimental unit ranged from 1 to 100 bars (calculated and additionally measured on a stand). The hydrogen pressure in the second experimental unit varied between 0.005 mbar (0.0037 torr) and 1.2 bar absolute pressure and had several cycles. Our idea was to trap hydrogen inside the reactor walls in impurities (such as twin boundaries and dislocations) that were introduced during the reactor manufacturing (caused by hammering, drilling holes, welding etc). This fuel was aimed at testing the results in [8]. Another idea was to use these reactors to test the idea of phonon excitation transfer, see the Discussion 4.1.
- Ni1 is the powdered form of Nickel that was obtained from the supplier as the crudest of all fuels used. Its purity is estimated between 75% and 90%. The oxidized surface was kept on purpose. The idea was that the oxidation being removed during the reactor operation. Such material could be used to trap hydrogen, again, in dislocations and twin boundaries that are formed around impurities in the material.

- Ni2 is Ni1 fuel that was pre-treated with hydrogen according to the table E1 that mimics the pre-treating, reported in [8]. After that, the fuel was loaded into reactors, never leaving hydrogen or inert atmosphere to prevent oxidation. The idea was to remove oxidation and pump out the resulting water vapor and other contaminating materials (restored by hydrogen pre-treating), thus maximizing the process of possible hydrogen trapping.
- Ni3 and Ni4 materials are basically purer (95% – 97%) and are used with the same reasoning as two previous materials, but have a finer grand. The pre-treating of material is performed analogously to processes reported in [8, 17] as well as with even more extensive procedures. The longest pre-treating during 8 weeks was performed for the Ni4 material. The original Ni3 material (oxidized, see figure J7) was gradually heated during one week up to the temperature of $250^{\circ}C$ in hydrogen atmosphere. It was then subject to cycles of vacuumization and hydrogen injection totaling 20 cycles withing a week with minimum hydrogen pressure of 0.005 mbar and maximum pressure around 10 bars. These cycles were repeated at temperatures $350^{\circ}C$, $400^{\circ}C$, $750^{\circ}C$. After the hydrogen pre-treating the surface of the material becomes clear but still maintains powdered form, see figure J8 for the example of the pre-treated fuel.
- Ni5 material is the Raney Ni that was manufactured from the Ni-Al alloy in place by the chemical process, see table E1. The idea behind this material is that it has the larges surface area of all considered materials (estimated $1gm$ has at least $0.5m^2$ of active area). If hydrogen can be trapped somewhere inside Ni material, then Raney Ni has a very good chance of trapping it. During preliminary experiments, the reactors with the Ni5 material substantially consumed hydrogen. An example of such hydrogen consumption and hydrogen trapping during pre-treating is provided in figure E1 along with the details.
- Ni6 material is a nano-Ni material that was obtained by exploding Ni-wires and was preserved in inert atmosphere by a team in Tomsk Polynech University. The idea behind this material was to verify the reports of several authors (including A.Rossi) that, presumably, used nano-Ni in their experiments. Possibly, such nanomaterial can mechanically interact with the surrounding materials, such as alumina, and trap hydrogen inside places of interaction. Ni6 material was either used as it is or pre-treated with hydrogen, analogously to the Ni4 material.
- Ni7 (PNK-UT1 20–60mkm) and Ni8 (PNK-OT2 40–100mkm) were the materials used by Parkhomov et al. in their experiments, see [17]. Those materials were also reported to the author during personal communications with A.G.Parkhomov as one of the most potent ones. They were pre-treated with hydrogen in the same manner as Ni4 material.

More informaiton on the fuel pretreaing is given in the Appendix E.

3. Results of experiments

All results were obtained by the execution of the provided Algorithm 1. At first the values of $K_j^e = 5$, $K_j^f = 1$ were used and later adjusted according to the previously observed results.

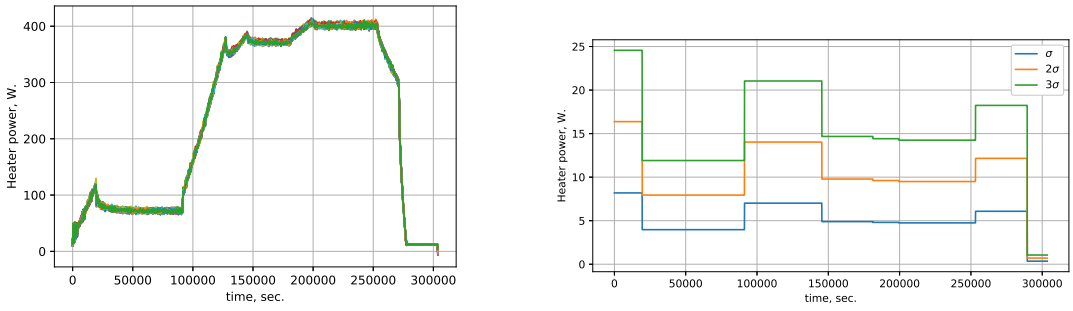

Figure 1. Heater power for all experiments on the first experimental unit with Π_1 (left), Levels of the standard deviation for the first set of axillary functions on all intervals (right).

Unfortunately, some regions of the programs failed the normality test and according to the Algorithm 1 step vi had to be re-executed. In this case, $K_j^e = 7$ and $K_j^f = 1$ or $K_j^f = 2$ were used for all j. The statistical analysis was performed according to the method described above in the subsection 2.1. In total, 43 statistical experiments for the first program Π_1, 15 statistical experiments for the second program Π_2 and 18 statistical experiments for the third program Π_3 were conducted during the research. Three more verification experiments were executed for Π_1 and Π_2. These experiments were used to estimate the sensitivity levels for all test units. These experiments included additional small heaters installed into reactors instead of a fuel with external small direct current power supply. The results of the verification experiments are considered below.

The standard deviations of the observed temperatures from the T_j^{set} are provided in the Appendix F, figures F1. The data is collected from all statistical and credible experiments. The variance is lower for the first experimental unit. This is expected since better thermocouples were used. The maximum errors in the controlled temperature are around 0.375% for $T \sim 400^{\circ}C$ level and around 0.17% $T \sim 1100^{\circ}C$ for the first experimental unit and around 0.48% for $T \sim 750^{\circ}C$ and 0.31% for $T \sim 1200^{\circ}C$ for the second experimental unit. The worst temperature error is in regions of initial heating and cooling for T_j^{set} (on the left) and those regions are excluded from statistical analysis. The observation temperature control is performed correctly and is stable with $\varepsilon = 0.5\%$. In absolute values, it means that the absolute maximum error is no more than $4^{\circ}C$ for the temperature around $1300^{\circ}C$.

The heater powers that correspond to all conducted experiments (both statistical and credible) are presented in figures. The results for the first experimental unit are presented in figure 1, for the second experimental unit in figures 2. The region of statistical experiments and statistical testing region are explicitly marked on these figures.

Possible heat production should be noticed as a drop of graphical representation of power consumption below such levels that this drop is considered statistically significant. The following subsections elaborate on the matter and provide information regarding sensitivity, uncertainty levels and statistical analysis of the results.

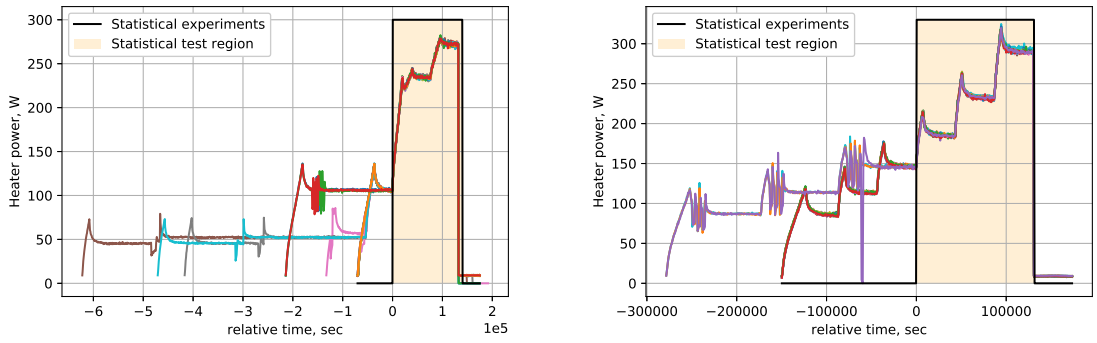

Figure 2. Heater power for all experiments on the second experimental unit with Π_2 (top) and Π_3 (bottom). Abrupt aperiodic change in power for $t < 0$ is due to vacuumizations and gas injections.

3.1. Statistical hypothesis testing, estimation of sensitivity levels

The collection of temporal intervals must be provided for each program Π_j, and it differs for different axillary functions used.

The intervals for (A.4) coincide with the programs intervals given in table 1 for Π_1, table 2 for Π_2 and table 3 for Π_3 for $t \geq 0$. For example, the following temporal intervals are used for Π_2: $[0, 20000]$; $[20000, 40000]$; $[40000, 76000]$; $[76000, 96000]$; $[96000, 132000]$.

The intervals for (A.5) are those intervals where the set temperature is kept constant. These intervals are also given by stages in T^{set} tables. The following intervals are used for Π_1: $[19440, 91440]$; $[145440, 181440]$; $[253440, 199440]$, for Π_2: $[40000, 76000]$; $[96000, 132000]$, for Π_3: $[7500, 43500]$; $[51000, 87000]$; $[94500, 130500]$.

3.1.1. First experimental unit The statistical hypothesis testing for the first set of axillary functions is executed on all intervals. Detailed information on the analysis of normality is provided in Appendix F.1.

The analysis of sensitivity is conducted with the use of verification experiment once the hypothesis of the normal distribution is accepted. The levels of standard deviations on each temporal interval are presented in figure 1. Notice, that the equation (A.3) is used to define the levels of the standard deviation, i.e. a maximum value of the deviation is used for each interval.

The resulting figure indicates 3σ level around 15W around $T \sim 1200^{\circ}C$ and around 22W for transitional stages. Initial and final stages can be excluded from the analysis. The verification experiment is analyzed in terms of the PID controller response to the change in the observed temperature, since the methodology is indicative.

The results are presented in figures 3 for the discrete calibration power supply signal and in figure 4 for the smooth calibration power supply signal. The graphs are presented in the deviation of the heater power from the main value in the left ordinate axis. The value of the calibration power is supplied on the right ordinate axis. The best results of detecting the

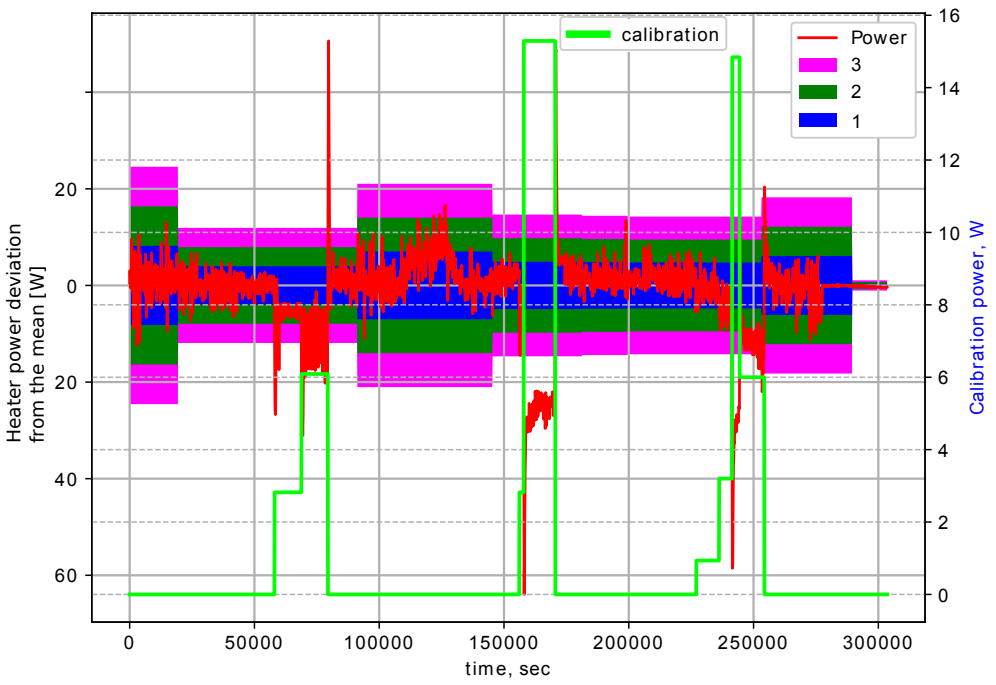

Figure 3. Calibration analysis of the heater power response for the discrete calibration power signal for Π_1.

heat production by the calibration heat source are observed for the discrete calibration power signal. The test (A.1) in the algorithm 1 fails at the calibration power levels $N_{cal} > 5$ W giving p at (A.1) around 6-8. A more precise sensitivity level estimate can be made using zoomed graphs for the smooth calibration experiment, these results are presented in Appendix G

The level of sensitivity of the experimental unit with the first set of the axillary functions in terms of 3σ can be estimated from the provided figures: $400°C - 3.5W$, $1200°C - 6W$, $1250°C - 5W$, which results in 4.8% for lower temperatures and 1.26% for higher temperatures in terms of the applied heater power.

The statistical hypothesis testing for the second set of axillary functions is described in Appendix F.1. The calibration is performed in the same manner as for the first set of axillary functions and the results of the smooth calibration with the controllable power supply at different intervals are provided Appendix G.

The smoothed data from the second set of axillary functions provides higher sensitivity. The level of sensitivity of the experimental unit with this axillary functions in terms of 3σ can be estimated from the provided figures: $400°C - 2.9W$, $1200°C - 3.85W$, $1250°C - 3.9W$, which results in 3.6% for lower temperatures and 1.05% for higher temperatures in terms of the applied heater power.

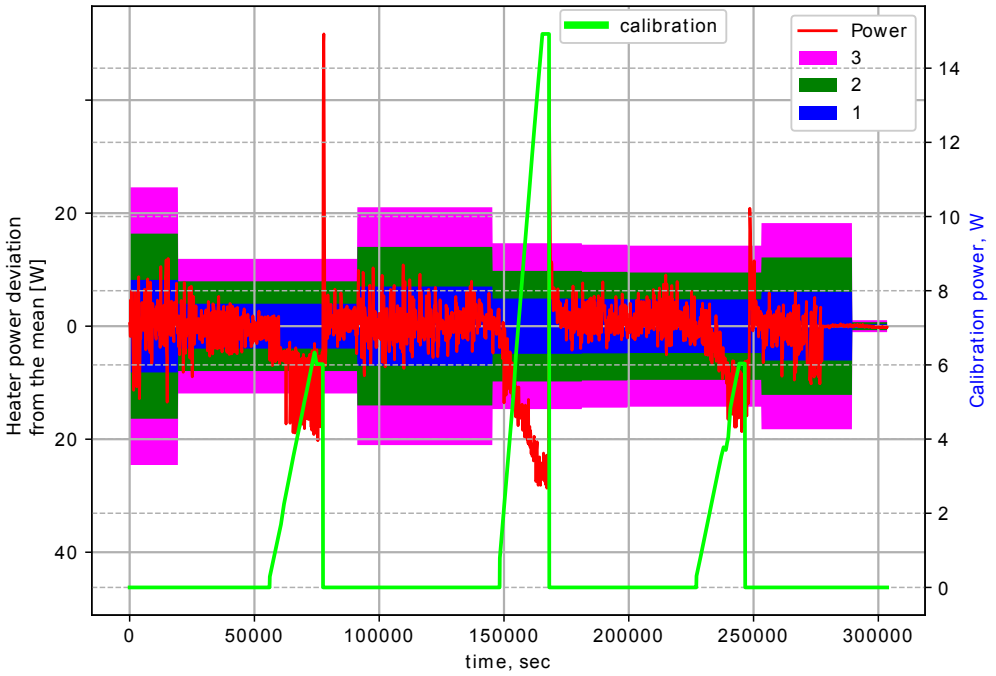

Figure 4. Calibration analysis of the heater power response for the smooth calibration power signal for Π_1.

3.1.2. Second experimental unit The same analysis for all intervals for the first and second set of axillary functions is described in Appendix F.2. The calibration analysis for the second experimental unit is performed only for Π_2 program as a discrete signal value on the verification heater. The results are presented in figure H1 and in Appendix H as the deviation of the heater power from the mean value for the first and second set of axillary functions.

The value of the calibration power is supplied on the right ordinate axis. Better sensitivity level can be estimated using the zoomed figure. The level of sensitivity of the experimental unit with the first set of the axillary functions in terms of 3σ can be estimated from the provided data as $3.0W$ at $1200^{\circ}C$. This results in 1.28% of accuracy in terms of the applied heater power for both sets of axillary functions.

Finally, one can conclude that the measured uncertainty is taken into account by the methodology, it is possible to accept the hypothesis of the normal distribution for the most of the data under the first set of axillary functions and for all intervals under the second set of axillary functions. The sensitivity levels for the first experimental unit are 3.6% and 1.05% for low and high temperatures, and 1.28% for the second experimental unit at high temperatures. Literally, it means that *excess heat power above 2.8 W at low temperatures and 4.2 W at higher temperatures can be confirmed in the first experimental unit and excess heat power above 2.5 W can be confirmed on the second experimental unit*. Any excess heat power which is lower than the thresholds but higher than the 2σ level can be observed during long tests,

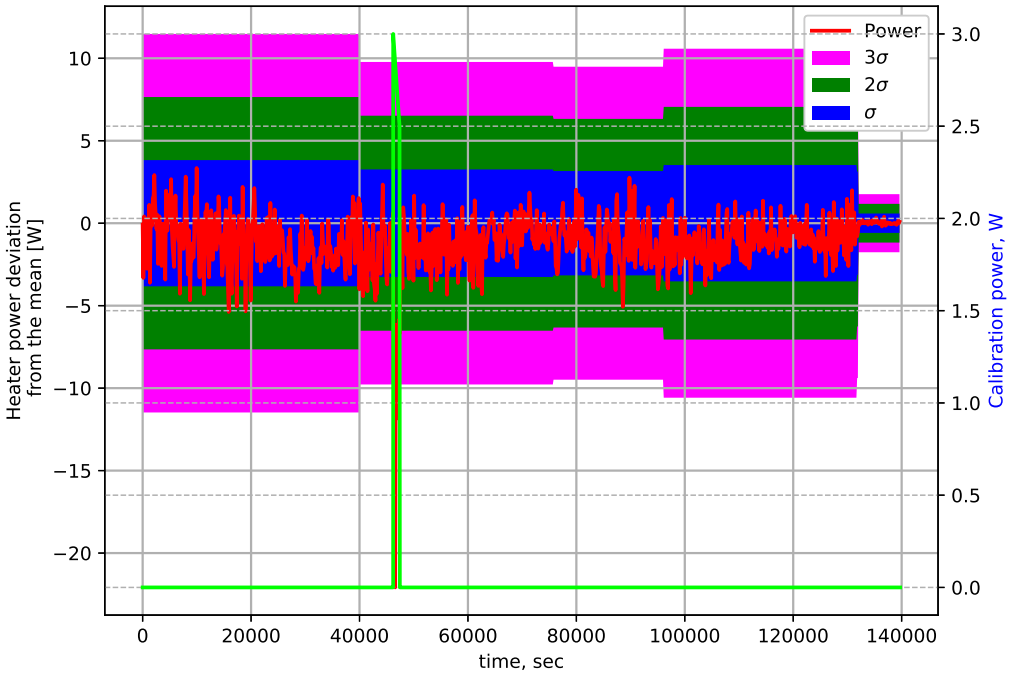

Figure 5. Calibration analysis of the heater power response for the discrete calibration power signal for Π_2, full interval.

but cannot be statistically confirmed.

3.2. Statistical analysis of credible experiments

It can be seen in figures 1 and 2 that no excess heat was detected during the experiments. This subsection includes more details on the matter once the statistical hypothesis are verified and sensitivity is estimated. It is important to note the test (A.1) failing for the negative heater power deviation, since one cannot be interested in lacking heat. Nevertheless, both tests are important, since the failing of the test (A.1) for the positive power deviation can indicate that the current experiment is not covered well by the performed statistical experiments.

3.2.1. First experimental unit The program Π_1 is considered. The analysis in terms of the first set of axillary functions is performed for all credible experiments brought together in figure 6.

Not a single credible experiment reached the 2σ level except at the beginning, where large deviations are due to transitional process. One can compare these results with figures 3 and 4 where calibration for the same program is presented.

The analysis in terms of the second set of axillary functions and Π_1 program is presented in the Appendix I.

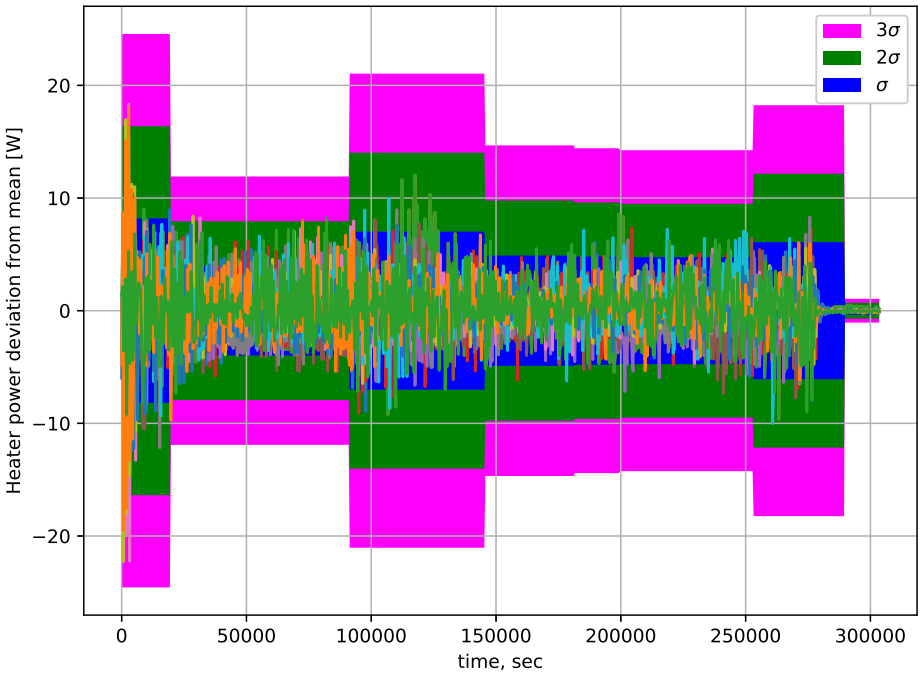

Figure 6. Statistical analysis of all credible experiments for the first set of axillary functions and Π_1.

The results indicate that all heater power deviation levels are well inside σ. The referenced calibration heater level gives a good estimate to the level of possible undetected excess heat. It can be concluded, that *no statistically significant levels of excess heat were produced during all credible experiments for* Π_1 *program.*

3.2.2. Second experimental unit The programs Π_2 and Π_3 are considered together. All credible experiments are again brought into single figures for the first set of axillary functions. Results are provided in figures 7.

All credible experiments produce heater power deviations well inside 2σ level. One of the experiments for Π_3 produced long term data in the upper deviation range above σ, which is statistically significant with the level around 34%. This is an indication that this particular experiment is not well covered by the statistical experimental series for Π_3. And this is indeed the case, since this particular credible experiment is number 10 in Appendix table E3. This experiment was tested with the Ni0 material sealed reactor, when all statistical experiments were conducted with open reactors. It was decided to avoid additional statistical experiments, since no excess heat was observed for this particular credible experiment in other regions.

The analysis in terms of the second set of axillary functions and Π_2 and Π_3 programs is presented in the Appendix I. First, all data for Π_2 lies in σ region, except for two or three outliers. But these outliers are well disproved by the main heater deviation level during

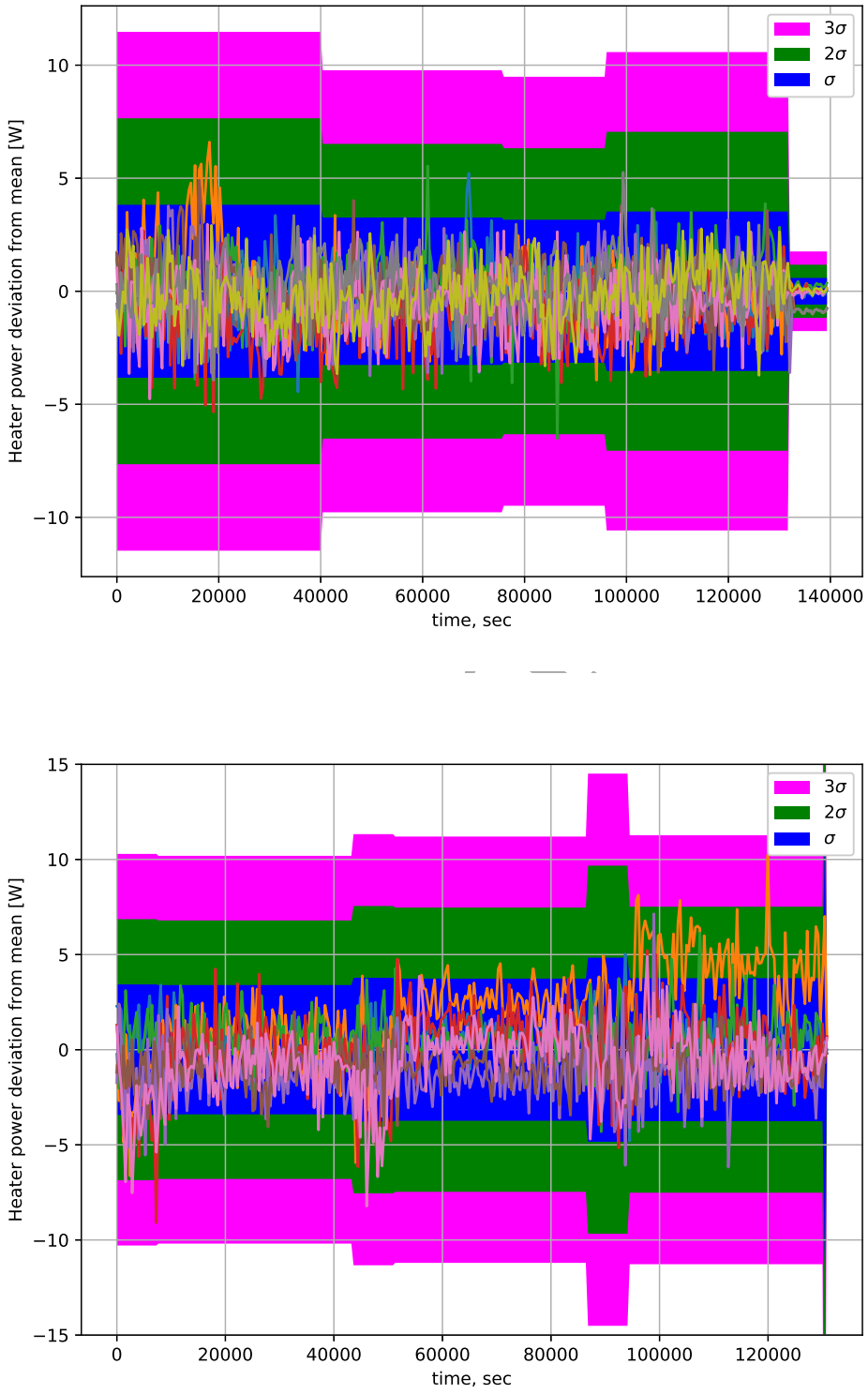

Figure 7. Statistical analysis of all credible experiments for the first set of axillary functions and Π_2, statistical analysis of all credible experiments for the first set of axillary functions and Π_3.

calibration experiment that has the lowest boundary, see figure I2 in Appendix I. Second, it is confirmed that the experiment number 10 with the Ni0 sealed container is not covered well in statistical experiments, see figure I3. However, its deviation is positive and, hence, no excess heat was generated. This also proves that the second set of axillary functions is more sensible. The final conclusion is that *no statistically significant levels of excess heat were produced during all credible experiments for* Π_2 *and* Π_3 *programs*.

4. Discussion

4.1. Possible reasons for failing the excess heat production

First, we would like to discuss why we failed to replicate excess heat production in Ni-H and Ni-D systems. One possible reason is that some specific features were not taken into account during the fuel selection, fuel pretreating and experimental execution. We tried to cover as much possible experiment protocols as we could. In order to do so, we made some personal communications with some authors of cold fusion experiments, including A.G.Parkhomov, in terms of fuel components selection and fuel pretreating protocols, see subsection 2.5. Our mistake in this part can only be due to some proprietary information that was kept from us (however, not likely). The protocol of all experiments was based on seven principles listed in the Introduction Section, Problem Formulation Subsection 1.2. As can be seen from the provided programs (tables 1, 2 and 3) and protocols, we tried to mimic the other authors experiments without violating the listed principles. This can be a problem, but whether this problem is related to some specific cold fusion ingredients missing or more precise experiments conducted with minimized FPs is not for us to judge.

In an attempt to cover all possibilities, we tested both Hydrogen and Deuterium as pure gases as well as Hydrogen - Deuterium mixture of $10:1$. It is possible that one must use some other mixture ratio in order to see the effect of the heat production.

In order to test some ideas we also added radioactive decaying material (0.1g of uranyl nitrate $UO_2[NO_3]_2$) in one experiment in three loaded fuels (Ni0, Ni4, Ni5) on the first experimental unit. The idea was to stimulate some degradation of material on the atomic level and perturb the lattice with external radiation (as much as we could). Our hypothesis was that such stimulation could allow us to trap more hydrogen and accelerate the formation of ultra-cold neutrons by the Widom-Larsen theory [26] by the induced radiation. This did nothing with the heat production, and that is why it is not explicitly mentioned in the section with the description of the used fuel.

Another idea, based on the theory of P.L.Hagelstein [22] (which hasn't being tested), was to excite phonons in nickel samples to achieve the phonon-mediated nuclear excitation transfer. It was planned to use the difference in thermal expansion coefficients of stainless steel alloy KhN-60VT and Nickel (which varies as 12.7 – 16.8 $[10^{-6}/grad]$ for temperature $100°C$ – $1000°C$) and steel alloy G13 which is the Russian analogue to the Hadfield steel (thermal expansion coefficient 18 – 23.2 $[10^{-6}/grad]$ for the same temperature range). The construction assumed a nickel torus being placed in the stainless steel reactor (cylinder with

a whole in the middle). Inside this torus, a tightly fitted stainless rod made of G13 alloy is inserted (tight-fitting by preliminary cooling of the rod). The whole setup is placed into the external reactor. Once the pretreating process is complete (at temperatures no more than $250^{\circ}C$) the credible experiment begins. Due to the difference in thermal expansion coefficients and mechanical properties of the G13 alloy, the central rod starts to push the nickel torus outwards. Directional phonons are formed on the contact surface as the result of the induced mechanical stress. It was planned to use Ni0 material (reactor wall itself) as the nickel sample. Unfortunately, this experiment was never finished due to the budget cutting, so we can assume that this can be another road to perform test experiments. On the other hand, it is not clear how narrow spectra phonons are being exited in other Ni-H and Ni-D experiments with powdered nickel fuels. The usage of H-D mixture was also partially inspired by the ideas of P.L.Hagelstein about a possible H-D synthesis in the condensed matter lattice structures.

4.2. False positive result

It is instructive to provide one False Positive (FP) result that occurred at the early stage of research. This result was partly the inspiration for the principles listed in the Subsection 1.2 and was obtained during the early stage of the experimental unit engineering. On this stage, the design of the first experimental unit had six reactors instead of three and there was no reactor thermal radiation cover, which is designated "2" in figure C2. The observation thermocouple was installed in the middle between these six reactors, i.e. in the middle of the gas chamber. The reactors could be heated through direct and scattered thermal emission, as well as could emit thermal radiation on the walls of the chamber and the observation thermocouple. This is a very tricky effect since it is nonlinear and depends heavily on the reactors surface emissivity.

The initial methodology hypothesis assumed that statistical experiments were to be conduced with the empty gas chamber (with no reactors installed), assuming that this was the case of the lowest energy consumption. The results of the first five experiments in terms of the heater power are presented in figure 8. The temperature in these experiments was subject to PID controlling under Π_1 program.

After the first assembly of the experimental unit, two experiments (number (1) and (2) in figure 8) were conducted to obtain statistical reference data. After that, six fuel loaded reactors were placed and tested as the credible experiment. The obtained result (number (3) in figure 8) indicated but didn't statistically justified possible excess heat. However, the situation was puzzling because monitoring thermocouples placed on the reactors showed ambient heater temperature close in values to the observation thermocouple. But if the reactor was the source of the extra heating energy, then the reactor thermocouples would show greater temperature values than the observation one.

In order to justify the initial methodology hypothesis, the next experiment was executed using new control reactors, shown by the curve number (4) in figure 8. It was noticed, however, that extracted reactors after two tests had different surface emissivity — fuel loaded reactors (experiment (3), figure 8) had darkened surface by the oxidation while control

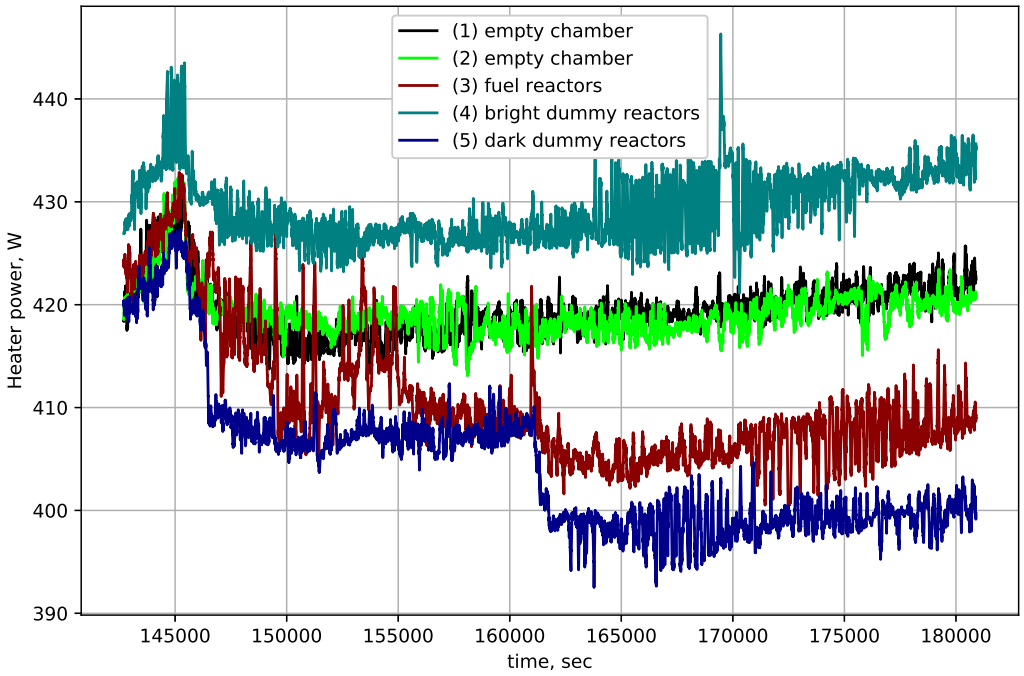

Figure 8. Heater power instantaneous data during first experiments with the altered first experimental unit construction. Program Π_1 is used, temporal interval $[142700, 181000]$ is shown, corresponds to $T^{set} \in [1170°C, 1200°C]$. Number in brackets indicates historical sequence of experiments.

reactors (experiment (4), figure 8) remained relatively bright. It was later learned that the thermal insulation in the first experimental unit was partially glued by high temperature glue that contained a small amount of water. This led to the oxidation for the fueled experiment (3) despite the inert atmosphere at high temperatures.

The reactor steel body is subject to hydrogen permeability. We believe that the result the following process took place: during heating the permeated hydrogen on the reactor surface restored the metal oxide until around $1050°C$. Then, the oxidation process intensified and the emissivity of the reactor surface changed, resulting in more intense re-emission of thermal radiation on the observation thermocouple. As the result, the temperature of the observation thermocouple was larger than that for the empty chamber.

To verify the influence of the reactor surface emissivity, another test with control reactors was performed. The surface of control reactors was darkened on purpose by the oxidation in the external heating device on the atmosphere. The next experiment number (5) disproved the assumed positive result of the credible experiment number (3) as can be clearly seen in figure 8. After this FP result was discovered, the construction of the first experimental unit was changed because of the noticeable influence of the emissivity. The reactor thermal radiation cover was added to prevent the possibility of such misleading results. The new unit was tested

again with both dark and light reactors and no significant differences were detected, hence, the effect of thermal radiation was eliminated.

This FP result demonstrates that even the slightest modification can lead to misleading results if highly nonlinear processes, such as thermal radiation, are not removed by clever engineered experimental units. The final item in the principles formulated in the Subsection 1.2 was inspired by the described FP result.

5. Conclusion

In conclusion, we would like to stress out that the paper doesn't cover the whole variety of Ni-H and Ni-D experimental protocols, and we don't want the readers to come away with the conclusion that Ni-H and Ni-D systems do not show anomalies under *any* conditions. Part of the work by Piantelli et al. was not covered [10], namely, the Ni-alloyed experiments. No nano-Nickel in complex forms in external matrices was tested, for example see the work of Takahashi et al. [27]. Obviously, the whole set of SRI experiments [2] and other experiments with co-deposited Ni are not covered by the current work, as stated in the introduction. The revision of these experiments was not perfomed because the funding was cut.

We encourage doubting researchers to replicate the above cited experiments with as much scientific rigor as possible, thus eliminating doubts. We believe that one should apply the experimental methodology based on the suggested principles (Section 1, Subsection 1.2) that we used in this paper.

[1] Berlinguette C, Chiang Y M, Munday J, Schenkel T, Fork D, Koningstein R and Trevithick M 2019 *Nature*

[2] Mckubre M 2015 *Current Science* **108** 495–498

[3] Hagelstein P L 2016 *J. Condensed Matter Nucl. Sci.* **20** 139–225

[4] Fleischmann M and Pons S 1989 *Journal of Electroanalytical Chemistry and Interfacial Electrochemistry* **261** 301 – 308 ISSN 0022-0728 URL http://www.sciencedirect.com/science/article/pii/0022072889800063

[5] Mills R L and Kneizys S P 1991 *Fusion Technology* **20** 65–81 URL https://doi.org/10.13182%2Ffst91-a29644

[6] Chechin V A, Tsarev V A, Rabinowitz M and Kim Y E 1994 *International Journal of Theoretical Physics* **33** 617–670

[7] Sheldon E 2008 *Contemporary Physics* **49** 375–378 URL https://doi.org/10.1080%2F00107510802465229

[8] Focardi S, Habel R and Piantelli F 1994 *F. Nuov Cim A* **107** 163 DOI:10.1007/BF02813080

[9] Campari E, S F, V G, Montalbano V, Francesco P, E P, Tosti E and Veronesi S 2000 *Ni-H systems* pp 69–74 ISBN 978-8877942562

[10] Campari E, S F, V G, Montalbano V, Francesco P and Veronesi S 2004 *ATTI DELL'ACCADEMIA DEI FISIOCRITICI IN SIENA* **XXIII** 47–58

[11] Ninno A and Frattolillo A 2008 *Historical Reconstruction of Cold Fusion activities at ENEA* ISBN 978-88-8286-204-6

[12] Levi G, Foschi E, Hartman T, Hoistad B, Pettersson R and Tegner L 2013 *Preprint at https://arXiv.org/abs/1305.3913*

[13] Levi G, Evelyn F, Bo H, Roland P, Lars T and Hanno E 2014 Observation of abundant heat production from a reactor device and of isotopic changes in the fuel URL http://amsacta.unibo.it/4084/

[14] Rossi A *Patent application WO2009125444A1*

[15] Clarke T 2015 Comment on the report "observation of abundant heat production from a reactor device and of isotopic changes in the fuel" by levi et al

[16] Ericsson G and Pomp S 2013

[17] Parkhomov A, Zabavin S, Timerbulatov T, Alabin K, Andreev S and Sobolev A 2017 *Radioelectronics. Nanosystems. Information Technologies* **9** 74–93

[18] Gorman J and Nardella W 1962 *Vacuum* **12** 19 – 24 ISSN 0042-207X URL http://www.sciencedirect.com/science/article/pii/0042207X62908217

[19] Toriyabe Y, Mizuno T, Ohmori T and Aoki Y 2006 *Condensed Matter Nucl. Sci.* **25** 253–263

[20] Mizuno T 2017 *J. Condensed Matter Nucl. Sci.* **25** 1–25

[21] Hagelstein P L and Chaudhary I U 2012 Coupling between a deuteron and a lattice (*Preprint* 1204.2159)

[22] Hagelstein P L 2018 *J. Condensed Matter Nucl. Sci.* **27** 97–142

[23] Evstigneev N M, Zaitsev F S, Klimov A I, Magnitskii N A and Ryabkov O I 2013 *Doklady Mathematics* **87** 354–356 URL https://doi.org/10.1134%2Fs1064562413030137

[24] Klimov A, Bityurin V A, Moralev I, Bychkov S, Pyatnitsky L, Tretyakova N, Evstigneev N and Ryabkov O 2014 Vortex control by pulsed power pumping *52nd Aerospace Sciences Meeting* (American Institute of Aeronautics and Astronautics) URL https://doi.org/10.2514%2F6.2014-0959

[25] Klimov A, Grigorenko A, Efimov A, Evstigneev N, Ryabkov O, Sidorenko M, Soloviev A and Tolkunov B 2016 *Journal of Condensed Matter Nuclear Science* **19** 145–154

[26] Widom A and Larsen L 2006 *The European Physical Journal C* **46** 107–111 URL https://doi.org/10.1140%2Fepjc%2Fs2006-02479-8

[27] Kitamura A, Marano E, Takahashi A, Seto R, Yokose T, Taniike A and Furuyama Y 2016 *Proceedings of JCF16*

[28] Field A 2013 *Discovering Statistics Using IBM SPSS Statistics* 4th ed (Sage Publications Ltd.) ISBN 1446249182

[29] Shapiro S S and Wilk M B 1965 *Biometrika* **52** 591–611

[30] Coin D 2008 *Statistical Methods and Applications* **17** 3–12

[31] Rahman M M and Govindarajulu Z 1997 *Journal of Applied Statistics* **24** 219–236

[32] The owen company for electronic hardware https://owen.ru/ [Online; accessed 23-Feb-2020]
[33] Li Y, Ang K and Chong G 2006 *IEEE Control Systems* **26** 42–54
[34] Gaodu A N, Pirogov A A, Gavrish A M and Drizheruk M E 1976 *Refractories* **17** 57–59 URL https://doi.org/10.1007%2Fbf01281714

Appendix A. The experimental methodology Algorithm

The experimental methodology itself is defined as the following formal abstract Algorithm:

Algorithm 1

(i) *Fix the set of programs* Π *for the given black box construction B.*

(ii) *Select a program* $\Pi_j \in \Pi$. *Set initial* $N^j := \emptyset$ *and* $Ng^j := \emptyset$, *define initial values for* K^e_j, K^f_j, *axillary variables* $K^e := 1$ *and* $K^f := 1$. *Set the desirable error* ε *in the observation parameter.*

(iii) *Select* $g \in F^j_B$.

(iv) *Perform statistical and credible (loaded with g) experiments to obtain the sets* $N^j := N^j \cup \{N^j_l(t_q)\}^{K^e_j}_{l=K^e}$ *and* $Ng^j := Ng^j \cup \{Ng^j_l(t_q)\}^{K^f_j}_{l=K^f}$, *for each discrete time point* t_q, $q > 0$. *Check that* $\|e_j(t_q)\| \leq \varepsilon$. *If this check fails, recalibrate the PID controller and goto i.*

(v) *Execute the uncertainty measurement and obtain the pointwise mean* E_q *and standard deviation* σ_q *for* N^j.

(vi) *Perform normality tests on the statistical population* N^j *on R intervals and check that the sample data are following a normal distribution. If normality tests fail, set* $K^f := K^f_j$ *and* $K^e := K^e_j$, *adjust* K^e_j *and* K^f_j *(if necessary), then goto iv.*

(vii) *Calculate functions* $\sigma := \sigma(\sigma_q)$ *over the pointwise standard deviation and* $\mu := \mu(E_q)$ *over the pointwise mean and function* $\mathscr{F}$ *over pointwise data. Select* $p \in \{1,2,3\}$, *and check, that*

$$\forall l = 1,..,K^f_j : n_g = \mathscr{F}(Ng^j_l)(t_q)$$

$$n_g(t_q) - \mu < -p\sigma, \forall q \in \bigcup_{r=1}^{R} [q^r_1, q^r_2]. \tag{A.1}$$

(viii) *If the test (A.1) fails for* $p = 3$, *define results of the credible experiment as "successful for g".*

(ix) *Set* $K^f := K^f_j$, $K^e := K^e_j$ *and desired* K^e_j, K^f_j *and goto step iii until all items in* F^j_B *are tested.*

(x) *Goto step ii until all items in* Π *are selected.*

This algorithm is executed for all black box constructions and all experimental programs. The points in the Algorithm 1 are further elaborated. By definition, measurement uncertainty is the expression of the statistical dispersion of the values attributed to a measured quantity. However, in order to use such definition, one must prove that a normal statistical distribution is valid in order to use dispersion and mathematical expectation based on statistical sample data. This point is checked in the Algorithm 1 at step vi. Couple of methods is included in the normality verification process. The first one is the visual quantile-quantile (QQ) plot test that is used for checking normality visually [28]. Then the histogram of values is presented with

fitted normal distribution on the histogram and estimation of the skewness (third standardized moment) and kurtosis (forth standardized moment) of the sample data. The other one is the statistical hypothesis test of Shapiro-Wilk [29]. It is based on the correlation between the data and the corresponding normal scores. This test is recommended for testing normality [28] even in the presence of outliers [30]. However, it is limited by the number of sample data and can't be applied for data sizes greater that 2000—5000 samples [31].

The pointwise mean value and standard deviation on step v of the Algorithm for the given set of intervals $\{[q_1^r, q_2^r]\}_{r=1}^R$ with $q_1^r < q_2^r, \forall r = 1, ..., R$ are defined as:

$$E_q = \sum_{l=1}^{K_j^e} N_l^j(t_q)/K_j^e, \tag{A.2}$$

and

$$\sigma_q = \left(\frac{1}{K_j^e - 1} \left(\sum_{l=1}^{K_j^e} \left(E_q - N_l^j(t_q) \right) \right)^2 \right)^{1/2}. \tag{A.3}$$

Three axillary functions in step vii of the Algorithm must be defined. Their definition relies on the fact that they must act on the pointwise data and must represent actual mean and standard deviation for μ and σ as well as actual data for $\mathscr{F}$.

In this research, two different set of functions is used (formally, most of these functions are functionals). The first one is defined by the following functions:

$$\begin{gathered} \mu(t_q) = E_q, \\ \sigma(t_q) = \begin{cases} \max\limits_{q_1^r \le q \le q_2^r} \sigma_q, \text{ if } q \in [q_1^r, q_2^r], \\ \text{undefined, if } q \notin [q_1^r, q_2^r], \end{cases} \\ \mathscr{F}(f)(t_q) = f(t_q). \end{gathered} \tag{A.4}$$

The μ – function is just a trivial function representing the pointwise mean value. The σ – function is the function that takes the maximum of standard deviations on the given interval $[q_1, q_2]$. If the condition (A.1) fails for (A.4) then it also fails for some $q \in [q_1, q_2]$ in (A.3) if the standard deviation is taken as a pointwise value. The data modifying function $\mathscr{F}$ is selected as a trivial one.

The second set of functions operates over the smoothed data. It is achieved by applying a cubic spline function $y(t) := SP(n(t_q), \kappa)$, where $n(t_q)$ is a discrete data and κ is the number of knots that are used in the spline function. The resulting values at discrete points t_q are obtained by the natural restriction, i.e. $y(t_q)$. The following functions are used:

$$\begin{gathered} \mu(t_q) = SP(E_q, \kappa), \\ \sigma(t_q) = \begin{cases} \max\limits_{q_1^r \le q \le q_2^r} \left(\dfrac{1}{K_j^e - 1} \left(\sum\limits_{l=1}^{K_j^e} \left(\mu(t_q) - N_l^j(t_q) \right) \right)^2 \right)^{1/2}, \text{ if } q \in [q_1^r, q_2^r], \\ \text{undefined, if } q \notin [q_1^r, q_2^r], \end{cases} \\ \mathscr{F}(f)(t_q) = SP(f(t_q), \kappa). \end{gathered} \tag{A.5}$$

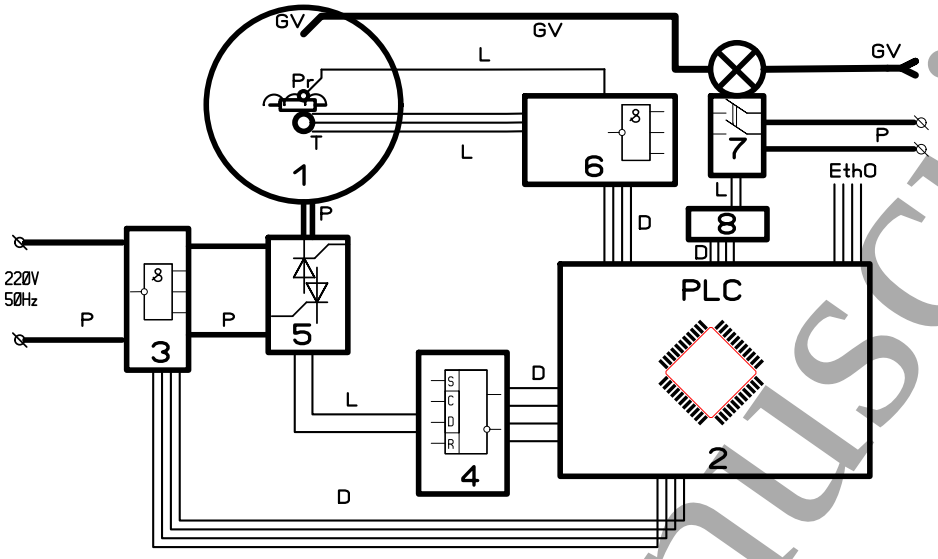

Figure B1. The main schematics of the experiment hardware and assembly: 1 - Experimental unit; 2 - Programmable logic controller; 3 - Digital power meter with ADC; 4 - Thyristor DAC; 5 - Thyristor power control block; 6 - measurements ADC; 7 - Block of electromagnetic valves, 8 - discrete DAC. 'P' denotes power grid lines, 'L' denotes low current analog lines, 'D' denotes low current digital lines, 'Eth0' is the Ethernet connection to a PC, 'T' is the thermocouples, 'GV' are the gas and vacuum lines and 'Pr' is the pressure gauge. Uninterruptible power supply unit and a PC are beyond the schematics.

Since the data is modified by the $\mathscr{F}$ in the second set of functions, it is also checked on the normality condition. It is done by considering the QQ-plots and construction of histograms with fitted normal distribution. However, in this case the whole interval $[q_1^r, q_2^r]$ is tested for normality. The utilization of different intervals given by $\{[q_1^r, q_2^r]\}_{r=1}^{R}$ allows one to exclude intervals of data with non-stationary processes or with wide range of deviations. The excluded data intervals are also excluded from the test (A.1) at step vii of the Algorithm 1 and are not taken into account during final conclusions.

Appendix B. The controlling and measuring hardware

The main schematics with experimental hardware and connectivity lines are presented in figure B1.

The hardware is based around the programmable logical controller (PLC) that controls all the peripherals and collects all measurement data, denoted "2" in figure B1. The OWEN PLC-150 [32] controller was used that contains RS-485 serial communication bus. It was used to communicate with DACs and ADCs over the digital signal "D" lines using MODBUS protocol with the communication speed 115200 bit/s. The connection to the computer (PC), running Linux OS, was established via the TCP protocol using the "Eth0" interface in figure B1. The PC sends a particular experimental program $\Pi_j \in \Pi$ that contains both temperature T^{set} and operation schedule to the gas and vacuum lines, as well as the desired coefficient vector $\mathbf{k}$ related to the PID controller. The PC receives the whole system operation status as well as

all measured and monitored data. The PC stores all data in the database format. The PLC is programmed using the CodeSys automation software for engineering control systems. The PLC contains a software implemented PID tunable controller that accepts control coefficient vector **k** from the PC. The PID controller implements the minimization of the error function (2) for each time t_q. The process of the PID tuning (determination of particular values in the vector **k**) is based on the well known method of Cohen-Coon and Ziegler-Nichols [33] and is beyond the scope of this paper. The obtained PID coefficient vector can be temperature dependent, i.e. $\mathbf{k}(T)$ thus one can robustly adjust the PID controller parameters depending on the temperature, if needed. Such PID tuning was performed for each construction of the experimental unit.

Initially, the hardware was designed to be used with the programmable stabilized direct current power supply. But this approach was abandoned due to the financial shortage, and thyristor control was used instead. This decreased the accuracy of the method slightly. The input grid power line is usually not stabilized for such controlling method with regard to the abrupt changes in the voltage withing the limit of 10–15%. In order to remove this uncertainty, a special function block was implemented that adjusted the PID controller level as a function of the input voltage in order to compensate for these abrupt changes in power grid voltage. It is based on the calculation of the power – PID controller level inverse function.

The observed temperature $T_j(t_q)$ as well as monitoring temperatures and pressure values (depicted "T" and "Pr" in figure B1) are transmitted via the low current signal in the shielded line "L" to the analogue-to-digital converter (ADC) "6" and then transmitted to the PLC "2". The PID controller generates the output digital signal that is transmitted via digital line "D" to the digital-to-analogue converter (DAC), denoted "4" in figure B1 that is specially designed to be used with thyristor controlling units "5". The ADC is the OWEN MB110-8AC with the 10-bit ADC and tunable parameters for particular thermocouples. The thyristor DAC is the 16-bit controller DAC and OWEN BOOST controller that accepts analogue 4-20mA low current signal and transforms it into thyristor controlling analogue signal. The measurement of the applied electric power is conduced with the ME110-224-1M (designated "3" in the figure B1) that has 0.5% maximum measurement error and 12-bit ADC. The module performs sampling of the current (maximum 5A) and voltage (maximum 264V) signals with the frequency of 150kHz and performs pointwise multiplication and averaging. Thus, the consumed power is estimated with no regard to the form of the input signal. The unit was tested against the oscilloscope measurements on different non-harmonic signals, and its performance was found satisfactory. Observe that the module is installed before the thyristor block, so the measured power includes the thyristor block own consumption (mainly due to the cooling system of thyristors and heating) that is around 10–12 W. This results in greater uncertainty level in the power signal but allows one to measure the unit performance from the grid. Note that all this uncertainty is automatically included into the interval of variance by the proposed methodology during statistical experiments. The gas and vacuum lines are controlled by the PLC via the electromagnetic valves "7" through the series of 1-bit discrete DACs "8" implemented by the solid state relays, see figure B1, according to the experimental program at hand.

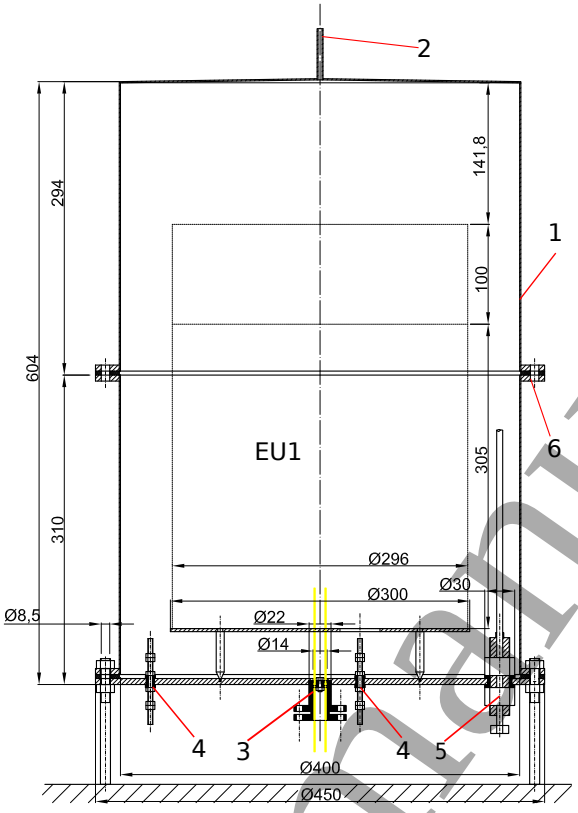

Figure C1. The assembly of the vacuum dome for the first experimental unit (EU1): 1 - top cover of the dome; 2 - pressure vacuum gauge sealed tube; 3 - vacuum sealed tube for the thermocouples line; 4 - vacuum sealed tube for the heater power line; 5 - gas and vacuum line; 6 - sealed dome main flange. All sizes are in mm.

The experimental unit is shown in figure B1 as ”1”; that is the object of observation, control and monitoring.

Appendix C. Experimental unit 1 – sealed reactors in the inert atmosphere

The main assembly consists of the dome that contains the experimental unit. The dome is vacuumed or filled with the inert gas (argon) during the heating. It also contains pressure vacuum gauge, electrical and gas lines that are vacuum sealed. The experimental unit schematics is given in figure C2 where the location of all elements is shown.

The Schupp ultra fiber board material is used for the thermal insulation that can operate up to the temperatures of $1600^{\circ}C$ without degradation. This material is based on the refactored ceramic fiber. It insures high durability, good thermal insulation and strength under limited reasonable loading. The thermal insulation is assembled using eight cylinders for the body and two cylinders for the top cover. Those cylinders are glued together by the high temperature glue. The highest temperature is around $150^{\circ}C$ on the outer side of the thermal insulation during the operation at maximum designed temperature at the control point. The design of the unit and initial PID tuning were numerically tested by the authors own CFD code.

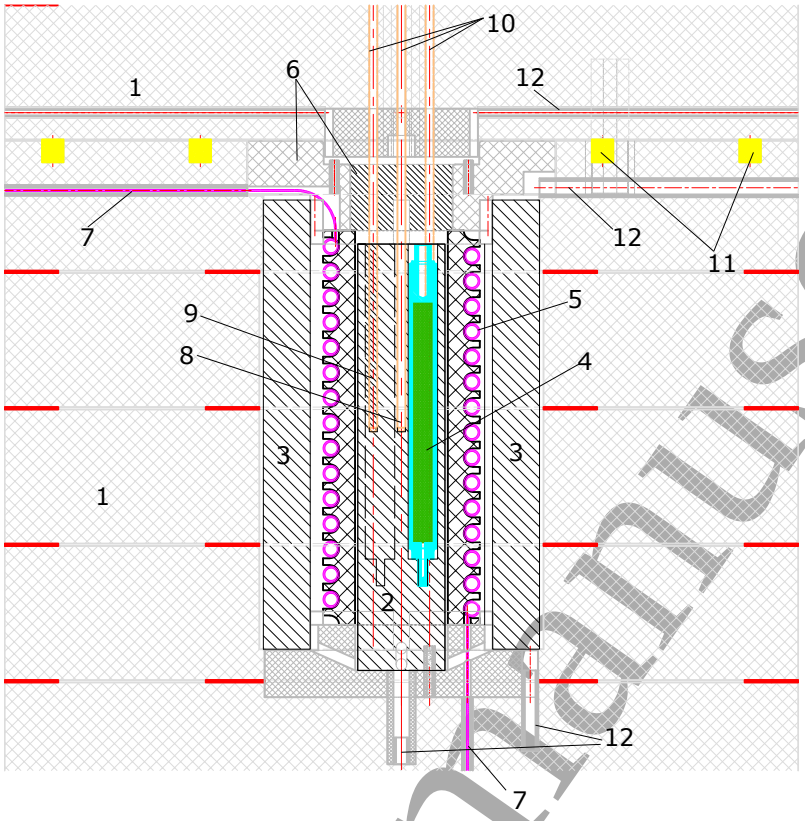

Figure C2. Schematic section of the first experimental unit: 1 - thermal insulation; 2 - reactors heat radiation cover (alumina); 3 - heater heat radiation cover (alumina); 4 - sealed reactor; 5 - heater; 6 - top reactors cover (alumina). 7 - heater power lines; 8 - observation thermocouple (PID-controller input); 9 - monitoring thermocouples; 10 - thermocouple channels (alumina); 11 - thermal insulation cover sealant; 12 - inert gas supply lines.

The heater is made of iron chromium aluminum (FeCrAl) alloy (russian code H27U5T) that has a working temperature up to 1350°*C*. The wire gauge is 1.2 mm^2 and is used in the form of a spiral with diameter of 5 mm, resulting in a stable long term operation in the inert atmosphere over a year. Three heaters were produced and calibrated in order to obtain uniform heating in case of the heater failure. The heater radiation cover made of alumina (”3” in figure C2) dissipates heat radiation and removes the nonlinear effects.

The type N (Nicrosil-Nisil) thermocouples covered in high temperature alloy containers are used with long term stable operation temperature up to 1300°*C*. The thermocouples are placed in precise positions by the guiding channels ”10”, see figure C2. This minimizes the spread of heater power when controlled by the PID controller.

The reloading process of the unit is the following, see figure C2. First, all thermocouples are removed from their channels ”10”. The top cover ”1” is removed and the reactor cover ”6” is lifted. The reactors are extracted from the reactor thermal radiation cover cylinder ”2”. Minimum deviations in the construction parameters are allowed during this process. After the reactors are replaced, the process is reversed. The thermocouples all have fixed positioning in the reactor thermal radiation cover ”6” so the measured points are always the same after the

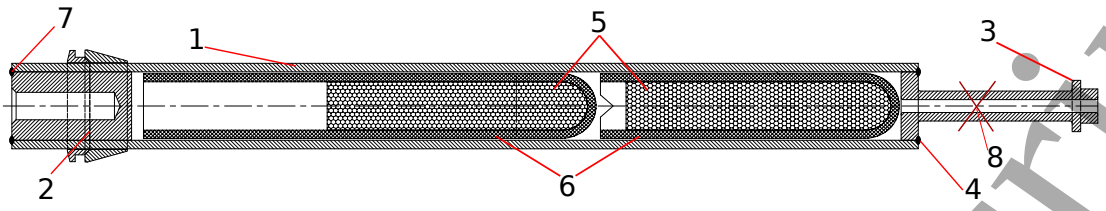

Figure C3. Construction of the sealed reactor: 1 - reactor body; 2 - top sealing cover; 3 - bottom gas filling tube; 4 - bottom welding; 5 - different fuel components (can be separated or joined) or alumina powder for control reactors; 6 - alumina opened test tube; 7 - top welding circle; 8 - place for the lower tube sealant. Orientation in the first experimental unit is vertical, in the second experimental unit is horizontal.

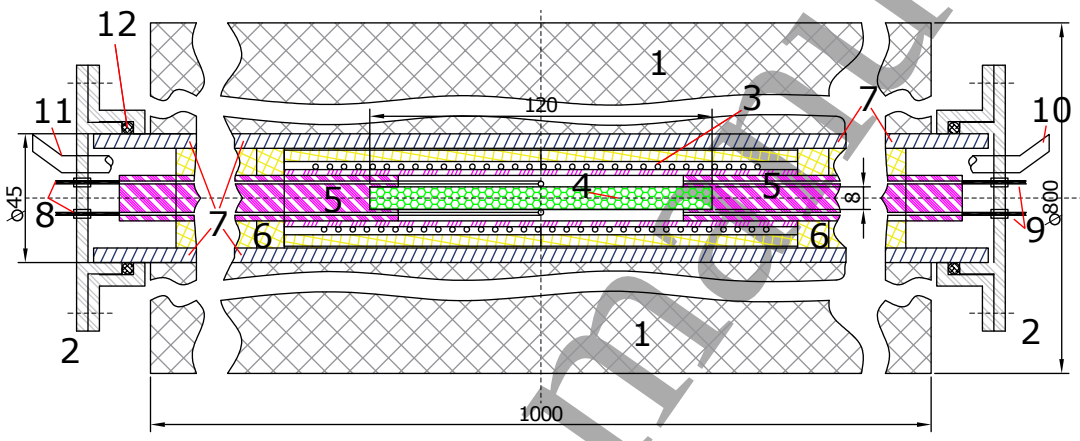

Figure D1. The schematic drawing of the second experimental unit (EU2): 1 - thermal insulation; 2 - vacuum sealed flanges; 3 - heater; 4 - open reactor; 5 - high temperature alumina cylinder with holes for wires; 6 - low density alumina for insulation of thermal radiation; 7 - high grade hydrogen proof alumina tube; 8 - vacuum sealed thermocouples lines; 9 - vacuum sealed heater power lines; 10 - gas and vacuum line; 11 - pressure vacuum gauge; 12 - vacuum and pressure sealant.

reload process is complete. One can notice that all nonlinear effects such as convection and thermal radiation are minimized by such design of the internal gas chamber.

The schematic of the sealed reactors used in this experimental unit are shown in figure C3. An example picture of the sealed and loaded reactors is provided in the Appendix J.

The reactor body was made of either Nickel or high temperature durable alloy KhN-60VT which is the russian analogue to the INCONEL 600 alloy. Such reactors can withstand long action of high temperatures. The hydrogen escapes these reactors during heating because of the hydrogen permeability through metals defined by the partial hydrogen pressure.

Appendix D. Experimental unit 2 – reactors in the hydrogen atmosphere

The schematic of the unit section is presented in figure D1. The design of the open reactor is given in figure D2. The picture of the unit and some internal parts are available in the Appendix J.

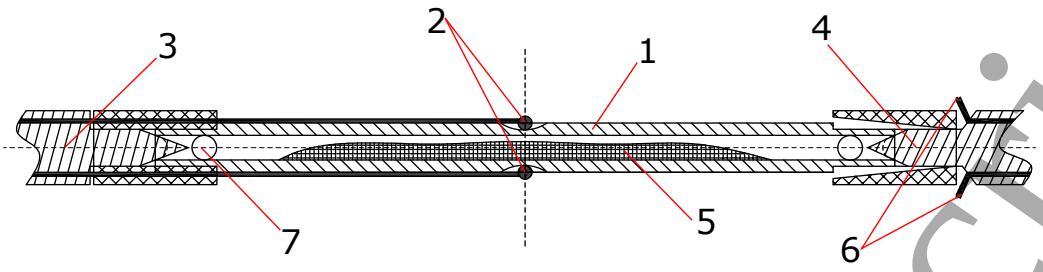

Figure D2. The schematic drawing of the open reactor and close construction for the second experimental unit (EU2): 1 - durable high temperature alumina reactor body; 2 - thermocouples; 3 - removable durable high temperature alumina cylinder; 4 - fixed durable high temperature alumina cylinder; 5 - fuel; 6 - heater power lines; 7 - gas ventilation opening.

The construction is designed in such a way that the internal part with the open reactor (left cylinder ”5” and open reactor ”4”) can be extracted through the left flange ”2” in figure D1. The kaolin wool [34] is used as the thermal insulation ”1” insuring high durability and fair insulating properties, resulting in the maximum external temperature on the outer side of the experimental unit around $100°C$ for the maximum internal temperature operation. The heater ”3” is made of the molybdenum wire of 1.0 mm^2 gauge shaped into a spiral, insuring stable operation up to $1600°C$ in hydrogen atmosphere. Low density alumina cylinders ”6” are used inside the tube to insure thermal insulation, preventing spread of the heat radiation and blocking convection. The asymmetric small diameter holes are made in those cylinders to insure gas permeability. The outer load bearing tube ”7” is made of high quality hydrogen tight alumina. The gas and vacuum lines are connected through the tube ”10” and the pressure vacuum gauge is attached to the tube ”11”. The flanges ”2” are attached to the tube by the sealant ”12” that insures vacuum and gas tight connection. The construction can withstand maximum absolute pressure up to 1.5 bars. The type C (tungsten/rhenium-alloy) thermocouples are used that can operate up to $2300°C$.

The fuel loading process is as follows, see figure D2. The flange in the left of the unit is removed. It removes the alumina bearing cylinder ”3” along with the attached open reactor ”1” that are connected to the flange. The reactor body contains guiding sockets for the thermocouples ”2”. The thermocouples are detached from the reactor. The fuel is loaded in the opening from both ends. Some fuel types can be covered with heptane or isopropyl alcohol in order to avoid oxidation. After that, the reactor body is attached to the bearing cylinder ”3” and the thermocouples ”2” are placed into the guiding sockets. The guiding sockets ensure that the temperature is measured at exactly identical points and this position remains fixed. The reactor ”1” along with the attached bearing cylinder ”3” is inserted back. The construction insures that the reactor is installed back in the same place by the guiding construction ”4” made of alumina. This part is not removed during the loading process and is located on the right in figure D1, number ”5”. The drilled openings ”7” in figure D2 provide the reactor internal part connection with the gas atmosphere or vacuum inside the chamber. If the fuel was covered with antioxidants, then these antioxidants are removed during the process of initial chamber vacuumation.

Table E1. Fuel components used for the credible experiments in both experimental units.

Designation	Fuel component	Comments
LAH	$Li[AlH_4]$	97% purity
Ni0	*Ni* cylinder 15mm	99.5% purity material for reactor production
Ni1	*Ni* 50mkm	powdered form, oxidised
Ni2	*Ni* 50mkm + H_2	powdered form, 4 weeks with 10 cycles of vacuum at temperatures from 350°*C* to 450°*C* in hydrogen.
Ni3	*Ni* 20mkm	powdered form, oxidised
Ni4	*Ni* 20mkm + H_2	powdered form, 8 weeks with 50 cycles of vacuum at temperatures from 250°*C* to 750°*C* in hydrogen.
Ni5	Raney *Ni*	powdered form, obtained from Ni-Al alloy by activating with concentrated solution of sodium hydroxide
Ni6	*Ni* 70nm	industrial powdered form, nano particles 160 – 50 nm obtained by electric explosion
Ni7	PNK-UT1 20–60mkm	powdered form, industrial, Ni 99.9% purity, used in [17].
Ni8	PNK-OT2 40–100mkm	powdered form, industrial, Ni 99.7% purity, used in [17].
H	H_2 gas	Electrolysis, 99.9999% pure.
D	D_2 gas	Electrolysis, 99.9999% pure.
DH	H_2 + D_2 10%mixture	Electrolysis, 99.9999% pure.

Appendix E. Fuel mixtures

The materials that were used as the fuel for credible experiments are presented in the table E1.

The set F_1^1 that corresponds to the first experimental unit $B = 1$ and first experimental program Π_1 is formed in tables E2. The sets that correspond to the second experimental unit $B = 2$ and two experimental programs are placed in table E3 and divided into F_2^2 for the Π_2 program and F_2^3 for the Π_3 program.

The third component in the first set is either nothing (the reactor is vacuumed) or gas (either hydrogen or deuterium) that fills the void. Two experiments number 7 and 13 use reactors that were made of pure nickel cylinder, material Ni0.

Table E2. The set F_1^1 of fuel combinations used for the credible experiments in the first experimental unit.

Expreiment No.	Comp. 1	Comp. 2	Comp. 3	Comment
1	Ni1	LAH	—	vacuumed
2	Ni1	LAH	H	
3	Ni2	LAH	H	
4	Ni3	LAH	—	vacuumed
5	Ni4	LAH	H	
6	Ni5	—	H	
7	Ni5	LAH	H	Ni0 reactor
8	Ni6	LAH	—	vacuumed
9	Ni6	LAH	D	
10	Ni7	LAH	H	
11	Ni8	LAH	H	
12	Ni8	—	DH	vacuumed
13	Ni5+Ni6	LAH	—	Ni0 reactor

Table E3. The set F_2^2, for numbers $1,..,9$ of the first program and set F_2^3, for numbers $10,..,16$ of the second program used for the credible experiments in the second experimental unit.

Expreiment No.	Comp. 1	Comp. 2	Comp. 3	Comment
1	Ni5	—	H	
2	Ni7	—	H	
3	Ni8	—	H	
4	Ni8	—	DH	
5	Ni8	—	D	
6	Ni2	—	DH	
7	Ni4	—	DH	
8	Ni5	—	DH	
9	Ni7	—	DH	
10	Ni5	LAH	H	Ni0 react
11	Ni2	—	DH	
12	Ni4	—	D	
13	Ni5	Ni6	D	50/50 mass
14	Ni8	Ni6	D	50/50 mass
15	Ni4	Ni8	D	50/50 mass
16	Ni5	Ni8	DH	50/50 mass

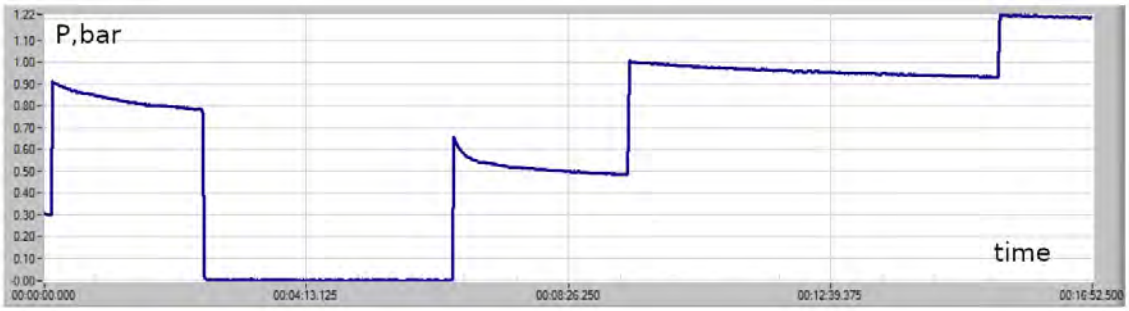

Figure E1. Absolute pressure vs time in hh:mm:ss.ms. Hydrogen consumption of the Ni5 material (Raney Ni) during testings on a stand. Total consumption estimated around 0.5 liters of hydrogen for $0.5gm$ of Ni5. Pressure drop from 00:03:15 to 00:06:45 is due to vacuumization in order to calculate residual hydrogen trapping. Residual hydrogen trapping estimated around 2–3% from the whole consumed volume during testings on the stand.

The loading of the reactors for the first experimental unit included four steps. First, one of the fuels from the set F_1^1 was loaded into the reactor in the inert atmosphere. After that, the reactor was locked by the top sealing cover and sealed mechanically in the inert atmosphere. On the second step, the reactor was attached to the cooling rack and the top of the reactor was welded. The cooling rack was automatically controlled so that the temperature of the reactor walls near LAH is lower than $40^{\circ}C$. On the third step, the inert gas inside the reactor was pumped out through the lower tube and then was filled either with selected gas (component 3 in table E2) or was kept under vacuum (appropriate comment in table E2). On the fourth stage, the lower tube is sealed and welded (again with temperature control) so that the fuel is sealed. The first experimental unit contained three reactors that could be tested at once, so all three were loaded with fuel in different proportions for credible experiments. This totals the number of credible experiments to 39 for the first experimental unit.

On the second experimental unit, the reactors have no sealing and the fuel is subject to the external gas, presented by the component 3 in table E3. Hydrogen injections and vacuumizations are performed in the same experimental unit for credible experiments. Only one sealed reactor was tested in this experimental unit, fuel number 10 in table E3. Some fuels for Π_2 and Π_3 programs were pretreated for 5-7 days. The pressure was monitored during this pretreating experiment, since sources like [17] and [8] reported pressure drop during heating below the level of atmospheric pressure. The pressure drop for Ni5 material (Raney Ni) is not anomalous, see above. We observed slight pressure drops below pressure atmospheric level during the process of fuel pretreating, but this can be interpreted either by hydrogen permeability through flanges or by the hydrogen diffusion into alumina.

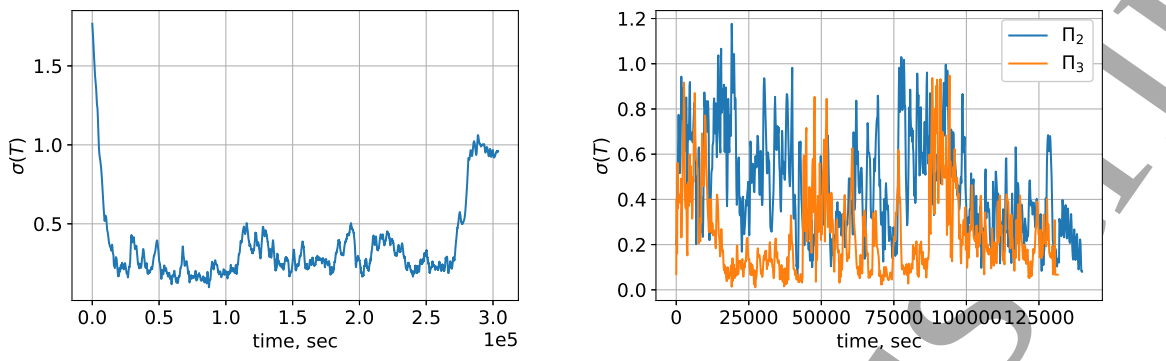

Figure F1. Pointwise standard deviations of controlled temperatures for all experiments on the first experimental unit with Π_1 (left) and for the second experimental unit with Π_2, Π_3 (right).

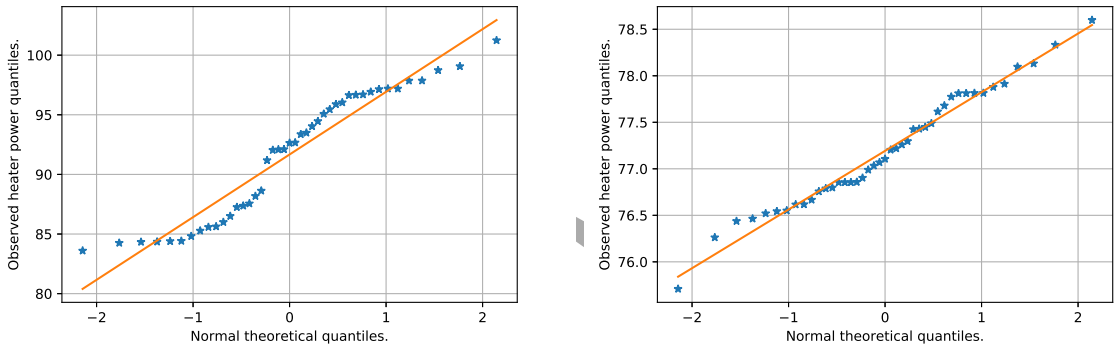

Figure F2. Worst (left) and normal (right) QQ-plot at the interval $[19440; 91440]$, $r^2 = 0.962$ for the first set of axillary functions.

Appendix F. Results of the statistical hypothesis testing.

Appendix F.1. First experimental unit

The Shapiro-Wilk hypothesis are satisfied at all intervals, except in the last interval where the power can be either 0 or 11 W, but this region is of no interest — the device is powered down at this region. This partly indicates that the sample population belongs to the normal distribution. However, some QQ plots show outliers, especially near the switch of temperature stages from linear increasing to the constant. Examples of the worst QQ plot and a standard QQ plot from one of the intervals are provided in figures F2.

Such poorly distributed quantile-quantile plots are located mainly near the points of stage changing in the set temperature program. The whole data, except for some points, can be accepted as normally distributed since all Shapiro-Wilk tests are satisfied and worst QQ plots are located on obvious singularities in derivatives in the temperature program. In addition, the average value of the r^2 parameter in the regression residuals in all QQ plots is 0.990, when the worst outlier value is 0.835. The QQ plots of the kind in figure F2 (left) are usually

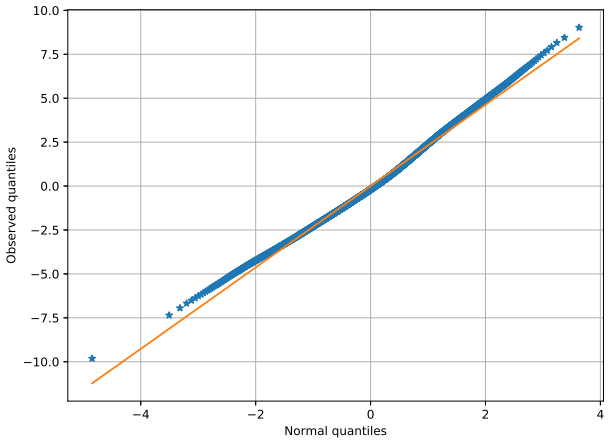

Figure F3. Cumulative QQ plot for $\mathscr{F}_2$ in the interval $[145440, 181440]$, $r^2 = 0.998$ for Π_1.

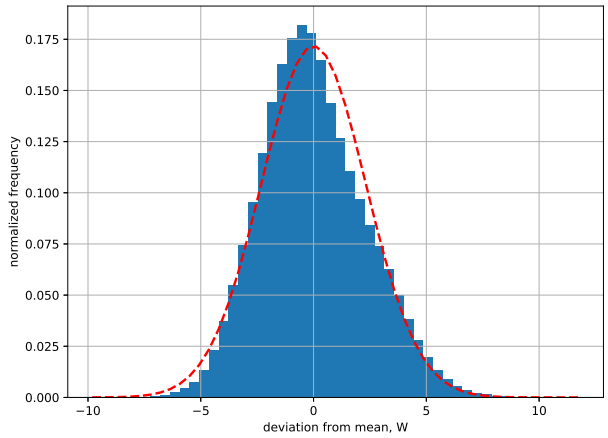

Figure F4. Cumulative histogram for $\mathscr{F}_2$ in the interval $[145440, 181440]$ with best fitted normal distribution by the dashed line, skewness = 0.303, kurtosis = 3.02 for Π_1.

suspected to have bimodal distribution. It is expected due to the change of the external experimental conditions. Such conditions depend on many random factors like deviations of temperature in the room, starting temperature of the experimental unit, average voltage level during the heating process etc. The manifestation of these changes usually presents itself near the singularities of derivatives in the T^{set} function. This can be cured by adding more statistical experiments, but authors had no such opportunity due to the termination of all experiments by the company. Some points where the QQ plot is substantially defected are discarded from the statistical analysis, totaling 213 points. This is approximately 0.1% of the whole sample data, which is acceptable. The hypothesis of the normal distribution is accepted for all other sampling data.

The statistical hypothesis testing for the second set of axillary functions is different and

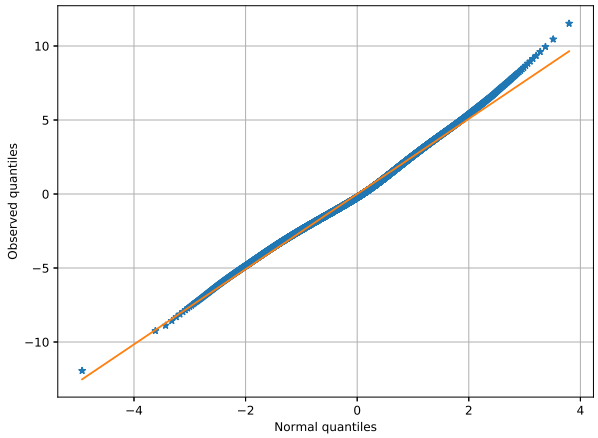

Figure F5. Cumulative QQ plot for $\mathscr{F}_2$ in the interval $[199440, 253440]$, $r^2 = 0.997$ for Π_1.

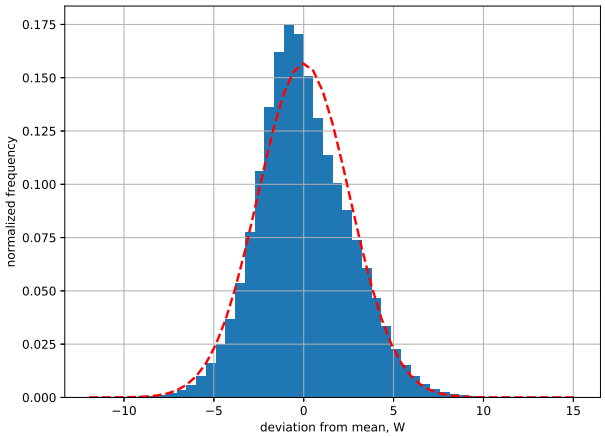

Figure F6. Cumulative histogram for $\mathscr{F}_2$ in the interval $[199440, 253440]$ with best fitted normal distribution by the dashed line, skewness = 0.258, kurtosis = 3.29 for Π_1.

follows the procedure described above in subsection 2.1. For all intervals, a spline with 17 knots was found to be optimal, so $\kappa = 17$ is taken in (A.5). The cumulative QQ plots for all intervals indicate almost perfect normal distribution, for example see figure F7, left. The resulting skewness is -0.047 and kurtosis is 2.74. The histogram with the best fitted normal distribution is provided in figure F7, right. Other results of QQ-plots, values for the higher statistical moments and histograms are provided in the figures below. For all these intervals, one can conclude that the hypothesis of the normality is satisfied.

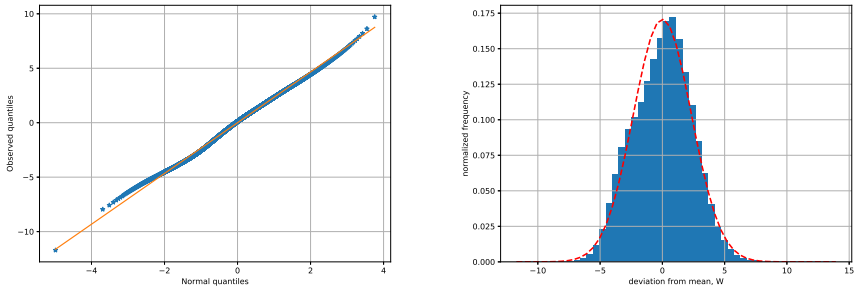

Figure F7. Cumulative QQ plot for the second set of axillary functions in the interval $[19440, 91440]$, $r^2 = 0.999$ (left) and cumulative histogram for the second set of axillary functions in the interval $[19440, 91440]$ with best fitted normal distribution by the dashed line (right).

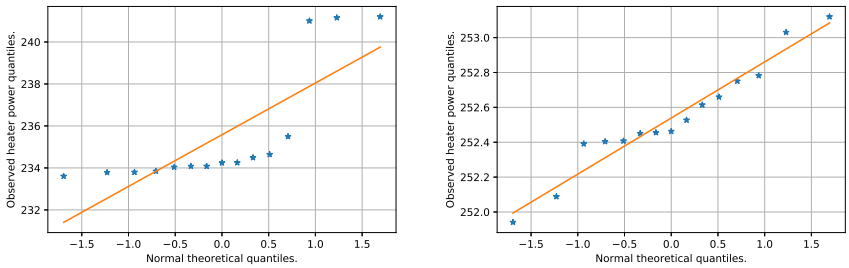

Figure F8. Normal QQ-plot at the interval $[96000; 132000]$, $r^2 = 0.943$ in Π_2 (right) and the worst QQ-plot at the interval $[96000; 132000]$, $r^2 = 0.872$ in Π_2 (left). All data for the first set of axillary functions.

Appendix F.2. Second experimental unit

Again, the situation is analogous to the first experimental unit. About 0.2% of all points for Π_2 and 0.15% for Π_3 are excluded from the statistical analysis due to defected QQ plots. The Shapiro-Wilk test is satisfied in all points, but points with defected QQ plots have p-values around 0.055 — 0.1. Examples of satisfactory and defected QQ plots are provided in figures F8.

The average value of the r^2 parameter in all QQ plots is around 0.941 for Π_2 and 0.969 for Π_3 and the worst outliers have r^2 values of 0.812 and 0.843, respectively.

The hypothesis of the normality can be accepted for the provided data, but on the lower level of acceptance than that for the first experimental setup. This is due to the lower number of statistical experiments being performed. The levels of standard deviations on each temporal interval are presented in figures F9 using the equation (A.3).

The substantial change in the standard deviation in the end of the Π_3 program is due to the different power-off times for different executions of the program, and this region is excluded from the statistical analysis.

The spline of 9 knots for Π_2 and 14 knots for Π_3 are used for the statistical hypothesis testing using $\mathscr{F}_2$ axillary function. The cumulative QQ plot in figure F10 together with the provided histogram and other figures in the Appendix F.2 for all other intervals shows that the distribution is close to normal but with lower assurance level than that for the first experimental unit. Such QQ plots indicate that the distribution contains so called "heavy tails" or, more precisely, the decay of variance is polynomial. This is also confirmed by the higher order statistical moments. The skewness is 0.12 and kurtosis is 4.45 for the provided QQ plot in figure F10.

The situation is better for the Π_3 program since more statistical experiments were conducted during the execution of the Algorithm with this program, see figures in the Appendix. So the hypothesis of the normality is satisfied for all intervals and both programs with lower levels than for the first experimental unit.

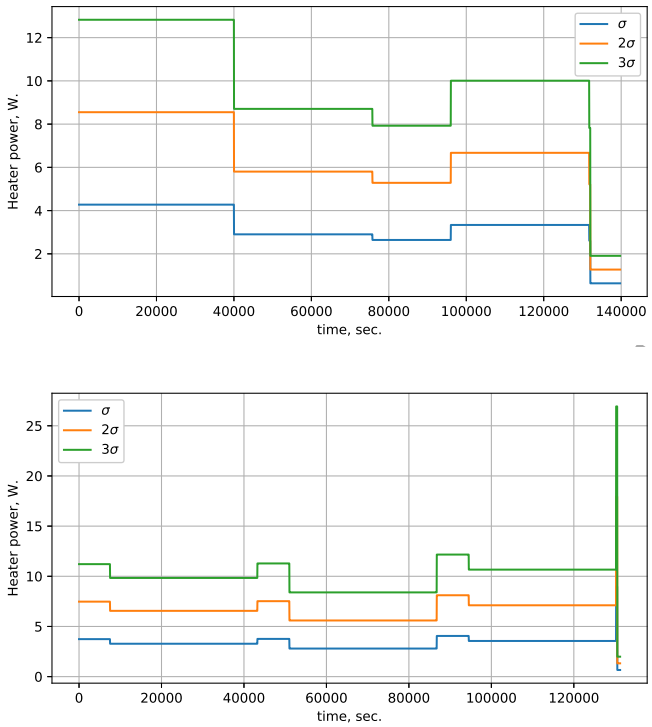

Figure F9. Levels of the standard deviation for the second set of statistical functions on all intervals for Π_2 and Π_3 in statistical regions.

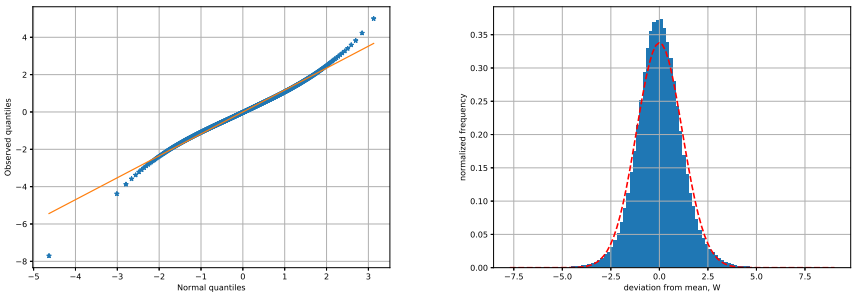

Figure F10. Cumulative QQ plot in the interval $[40000, 76000]$, $r^2 = 0.993$ for Π_2, left and cumulative histogram in the interval $[40000, 76000]$ with the best fitted normal distribution by the dashed line for Π_2, right. All data for the second set of axillary functions.

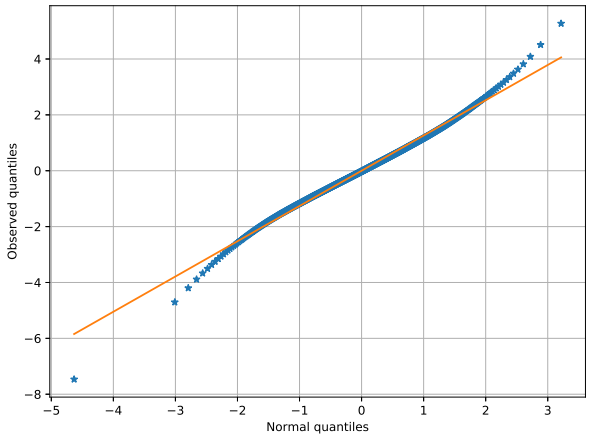

Figure F11. Cumulative QQ plot for $\mathscr{F}_2$ in the interval $[96000, 132000]$, $r^2 = 0.995$ for Π_2.

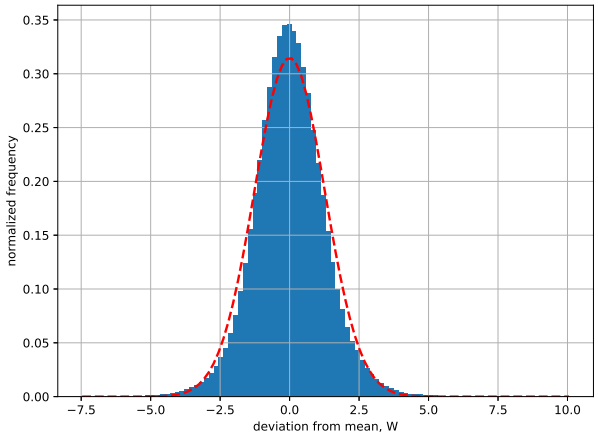

Figure F12. Cumulative histogram for $\mathscr{F}_2$ in the interval $[96000, 132000]$ with best fitted normal distribution by the dashed line, skewness = 0.065, kurtosis = 4.23 for Π_2.

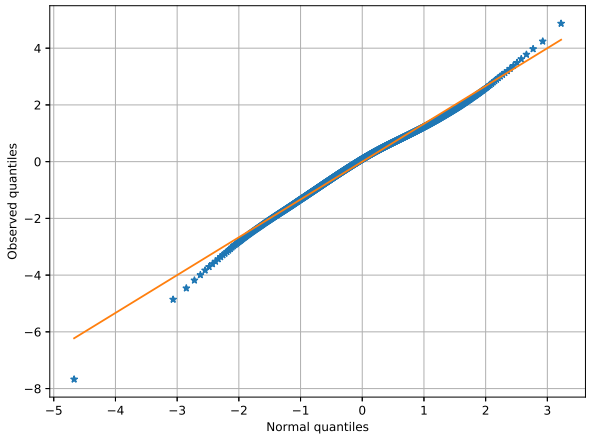

Figure F13. Cumulative QQ plot for $\mathscr{F}_2$ in the interval $[7500, 43500]$, $r^2 = 0.996$ for Π_3.

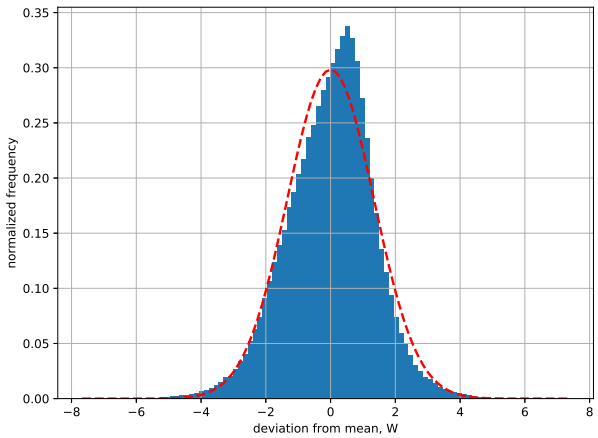

Figure F14. Cumulative histogram for $\mathscr{F}_2$ in the interval $[7500, 43500]$ with best fitted normal distribution by the dashed line, skewness = -0.20, kurtosis = 3.66 for Π_3.

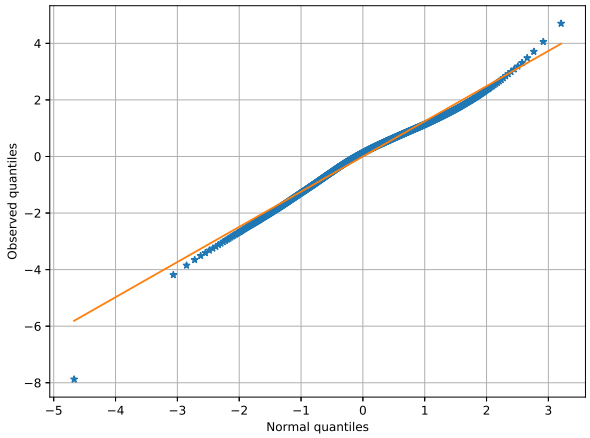

Figure F15. Cumulative QQ plot for $\mathscr{F}_2$ in the interval $[51000, 87000]$, $r^2 = 0.995$ for Π_3.

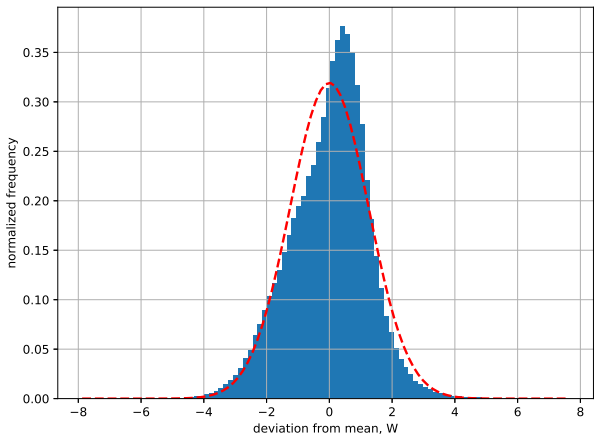

Figure F16. Cumulative histogram for $\mathscr{F}_2$ in the interval $[51000, 87000]$ with best fitted normal distribution by the dashed line, skewness = -0.22, kurtosis = 3.39 for Π_3.

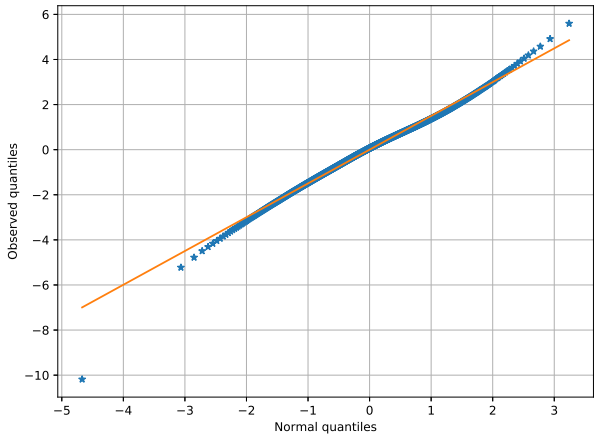

Figure F17. Cumulative QQ plot for $\mathscr{F}_2$ in the interval $[94500, 130500]$, $r^2 = 0.998$ for Π_3.

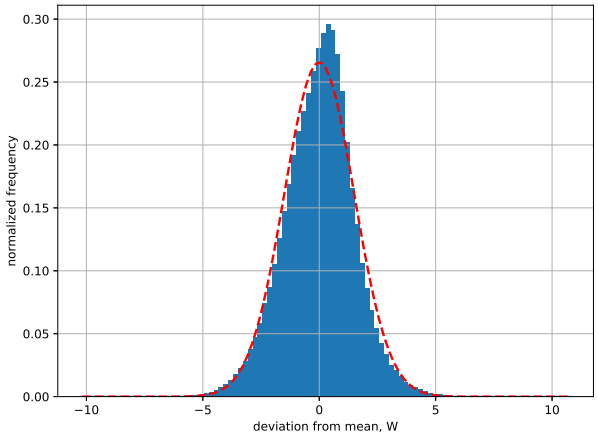

Figure F18. Cumulative histogram for $\mathscr{F}_2$ in the interval $[94500, 130500]$ with best fitted normal distribution by the dashed line, skewness = -0.09, kurtosis = 3.655 for Π_3.

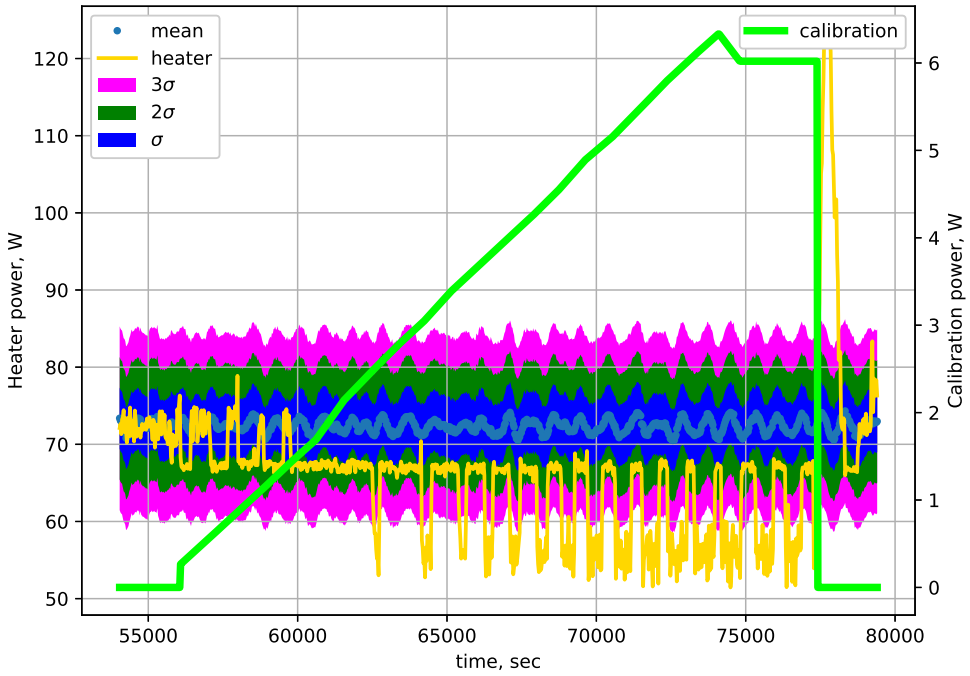

Figure G1. Calibration analysis of the heater power response for the smooth calibration power signal for Π_1 at $t \in [56125, 77500]$.

Appendix G. Zoomed in regions of the calibration experiments on the first experimental unit.

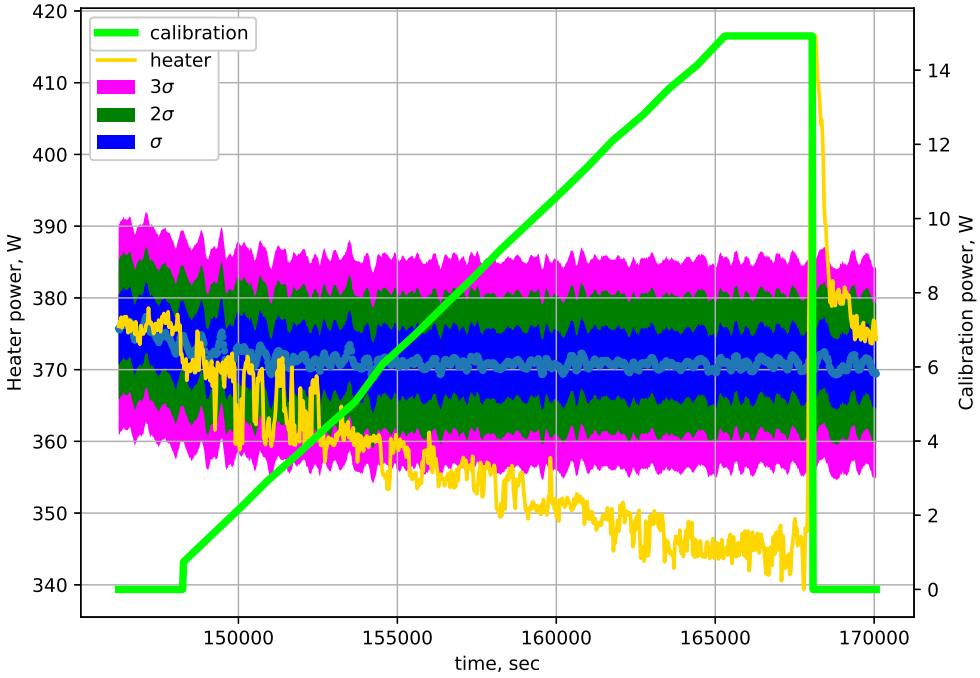

Figure G2. Calibration analysis of the heater power response for the smooth calibration power signal for Π_1 at $t \in [146125, 168000]$.

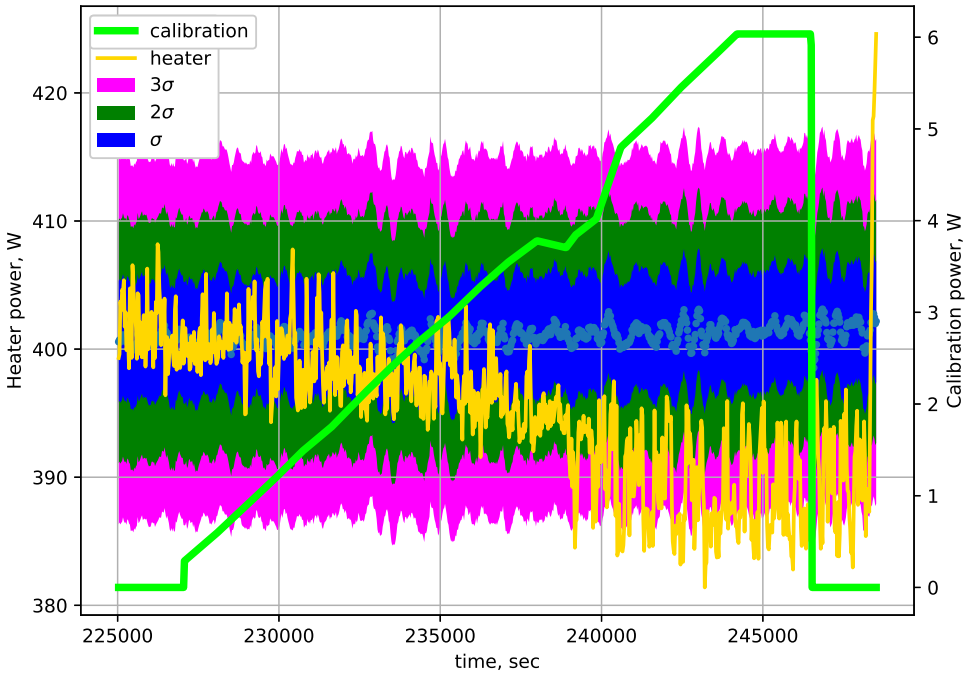

Figure G3. Calibration analysis of the heater power response for the smooth calibration power signal for Π_1 at $t \in [227000, 247250]$.

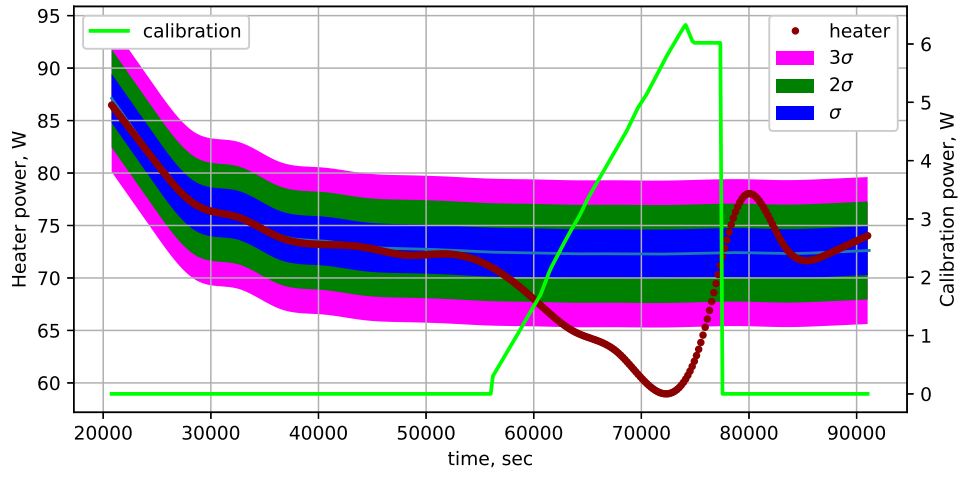

Figure G4. Calibration analysis of the heater power response for the smooth calibration power signal for the second set of axillary functions in the interval $[19440, 91440]$.

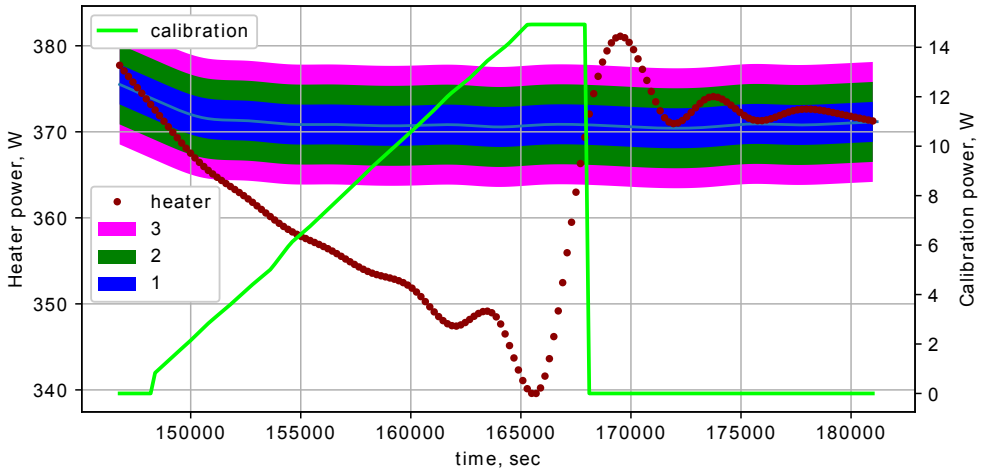

Figure G5. Calibration analysis of the heater power response for the smooth calibration power signal for the second set of axillary functions in the interval $[145440, 181440]$.

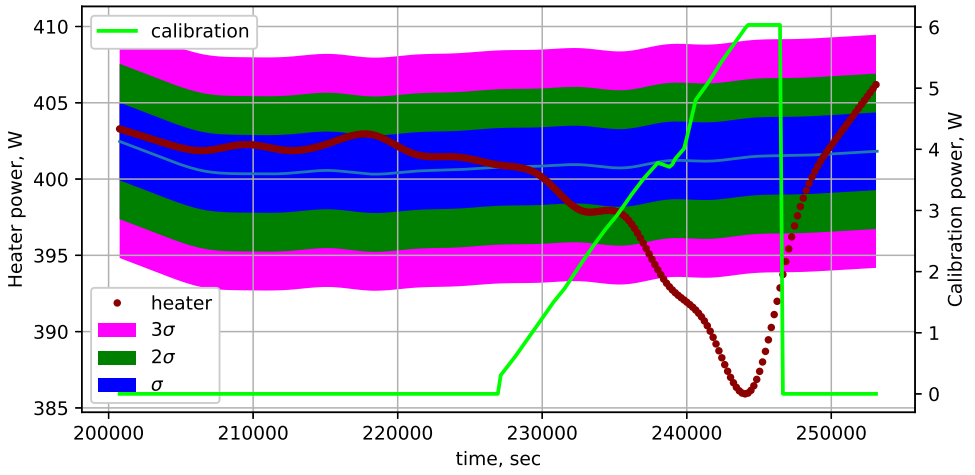

Figure G6. Calibration analysis of the heater power response for the smooth calibration power signal for the second set of axillary functions in the interval $[199440, 253440]$.

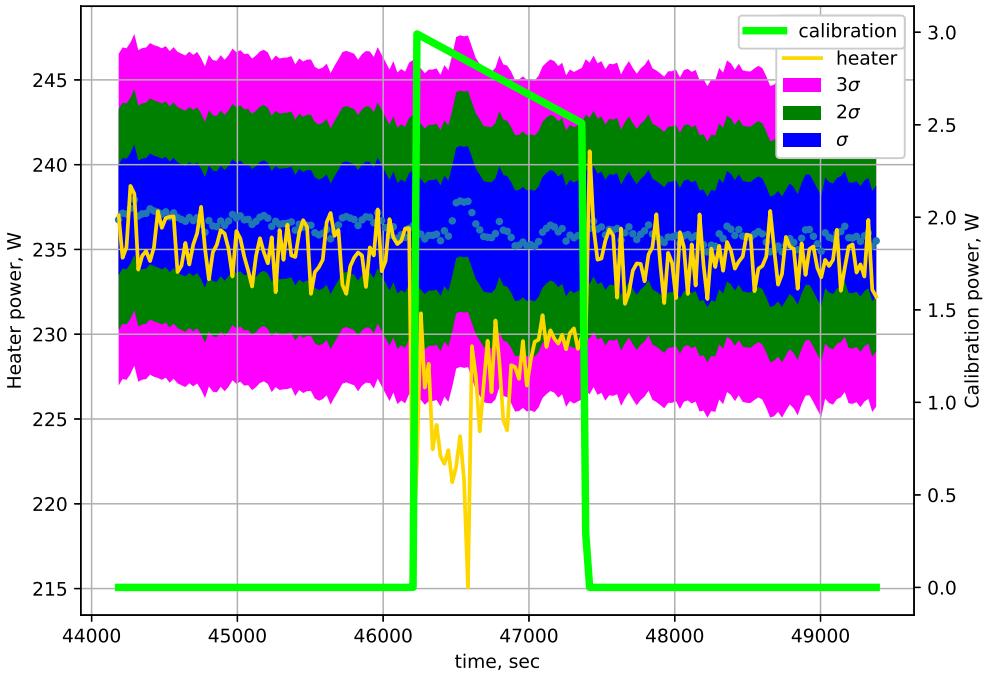

Figure H1. Calibration analysis of the heater power response for the discrete calibration power signal for Π_2, zoomed part. The value of the calibration power is supplied on the right ordinate axis.

Appendix H. Zoomed in regions of the calibration experiments on the second experimental unit.

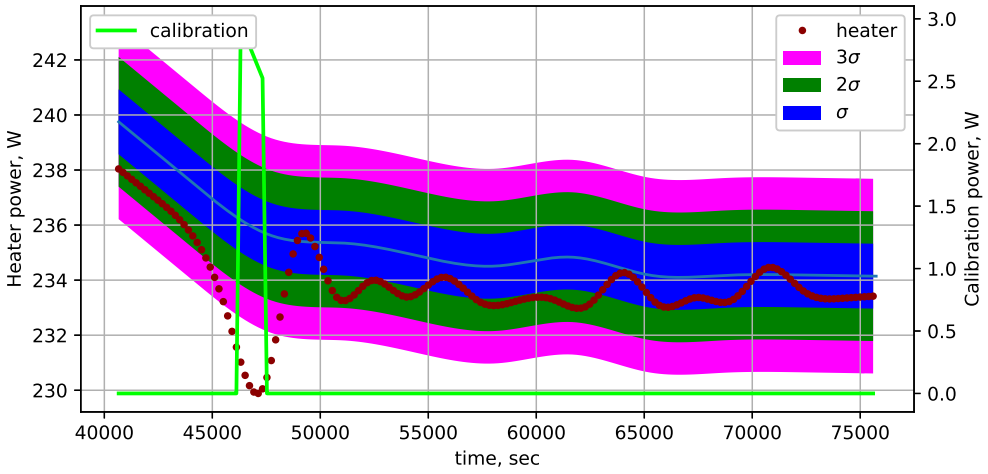

Figure H2. Calibration analysis of the heater power response for the discrete calibration power signal for the second set of axillary functions in the interval $[40000, 76000]$ for Π_2. The value of the calibration power is supplied on the right ordinate axis.

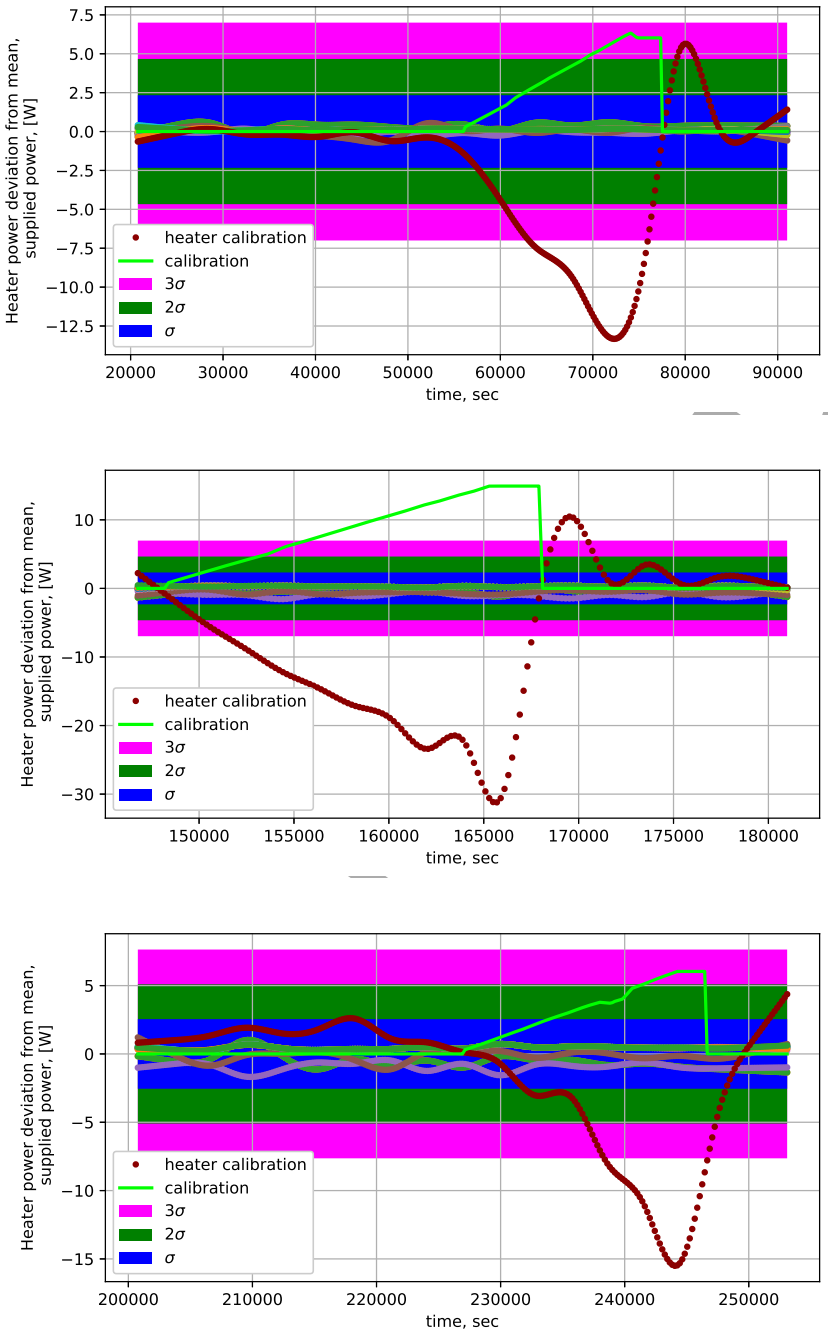

Figure I1. Statistical analysis of all credible experiments (colored curves) for the second set of axillary functions and Π_1 with added calibration results for reference.

Appendix I. Additional data for credible exeperiments.

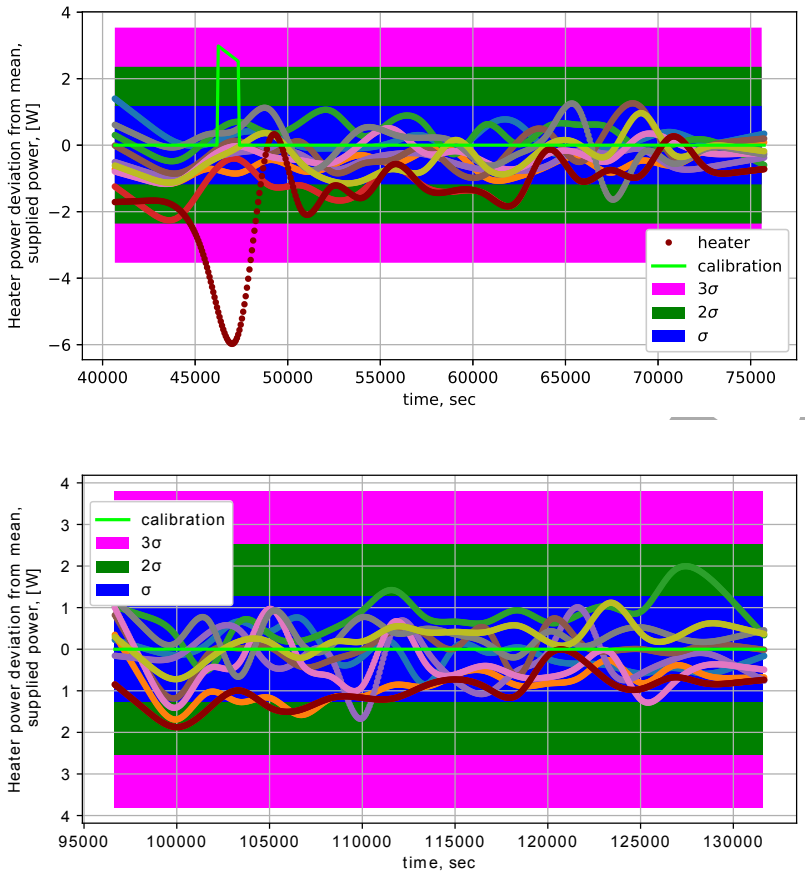

Figure I2. Statistical analysis of all credible experiments (colored curves) for the second set of axillary functions and Π_2 with added 3W calibration experiment for the reference.

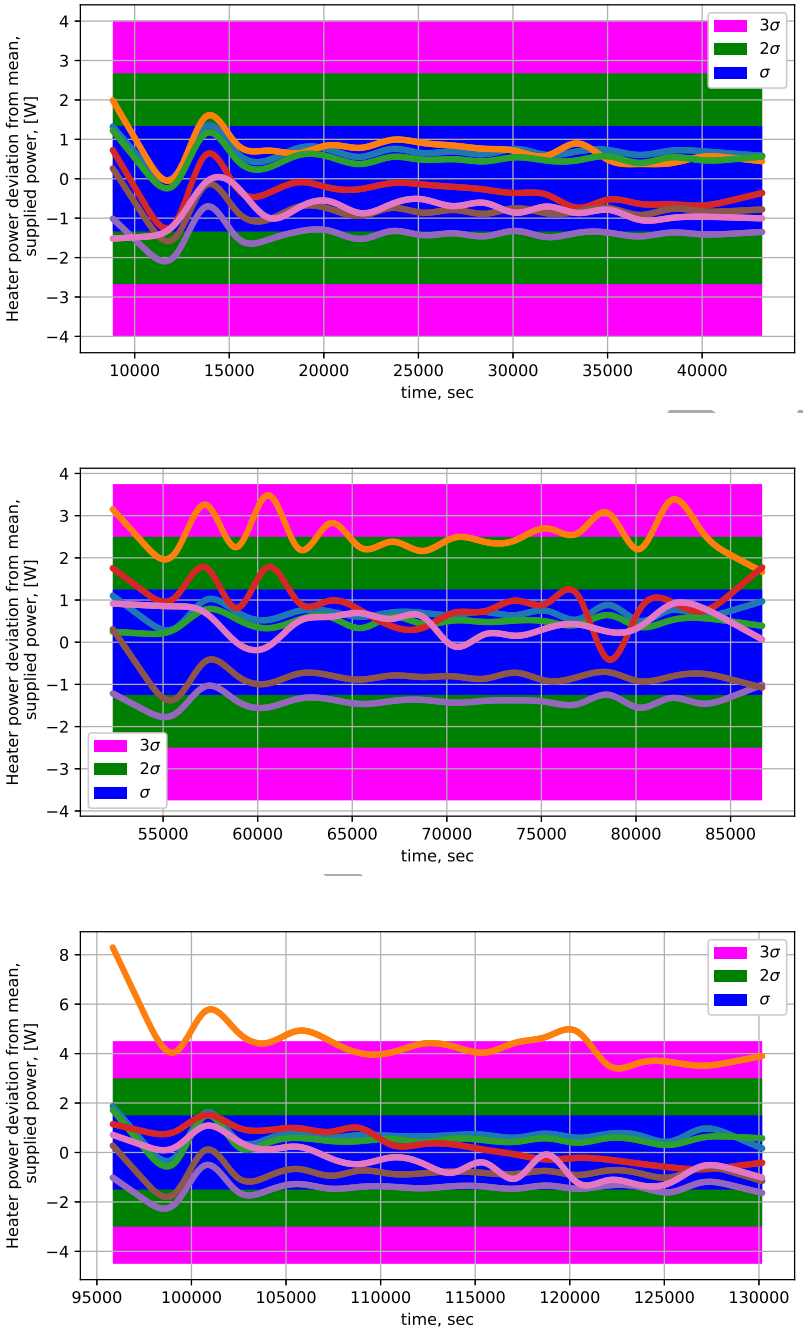

Figure I3. Statistical analysis of all credible experiments (colored curves) for the second set of axillary functions and Π_3.

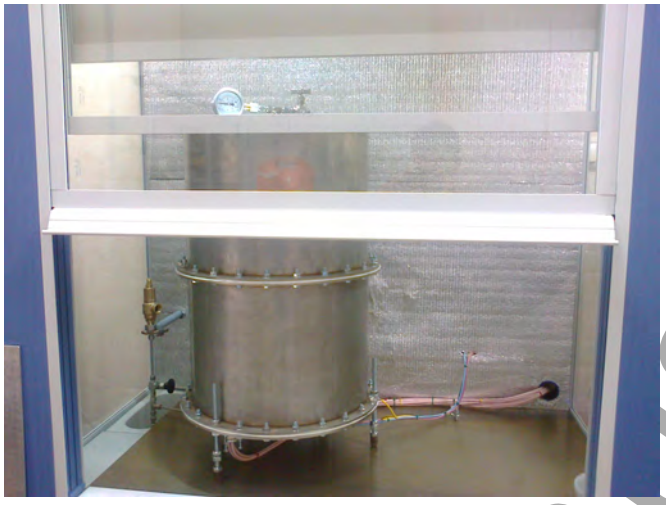

Figure J1. The general view of the first experimental unit. The main dome, shielded "L" thermocouple lines (pink), power lines "P" (yellow ground, read and blue) and gas and vacuum lines "GV" are visible.

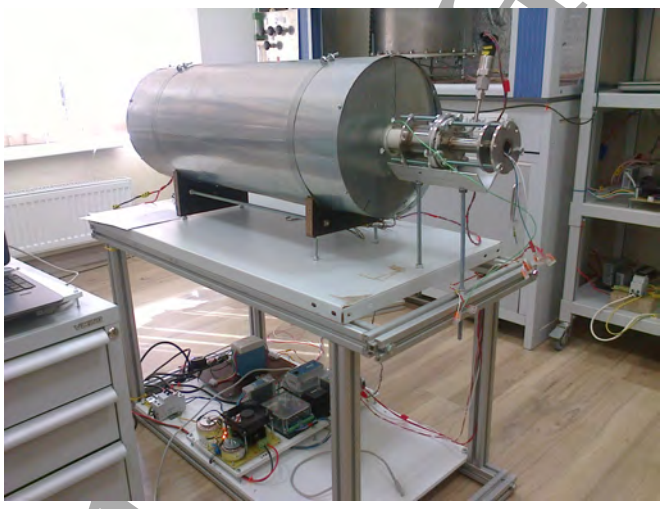

Figure J2. The general view of the second experimental unit in operation (1300°*C*) with the main electrical measuring and control hardware. Part of the first experimental unit and its measuring and control hardware is visible on the top and right

Appendix J. Pictures of the units, reactors and hardware

Figure J3. The internal part of the first experimental unit. One can see the flange of the dome, main cylindrical heat insulation, main loading gas chamber with heat radiation cover and three loaded reactors, isolating body and top cover of the heater.

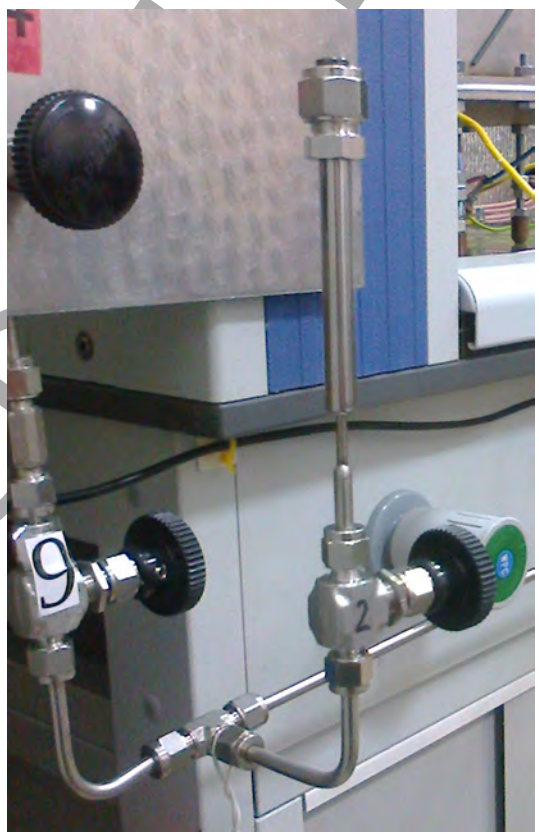

Figure J4. A sealed reactor with fuel is being vacuumed before the lower tube is sealed.

Figure J5. Prepared set of full and control sealed reactors.

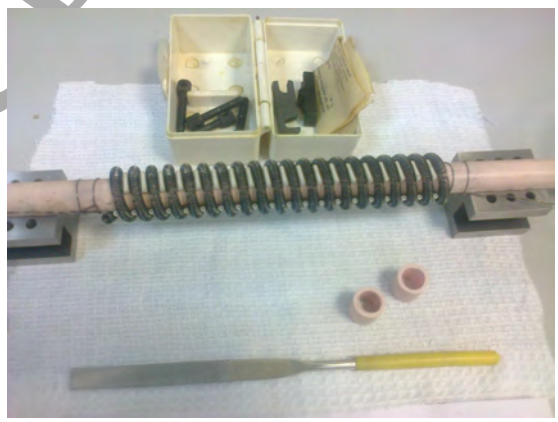

Figure J6. The molybdenum heater for the second experimental unit.

Figure J7. Example of Ni3 fuel. Oxide film is clearly visibly by the color. Compare with Ni4 fuel in figure J8.

Figure J8. Example of Ni4 fuel after being pretreaded with hydrogen and vacuumation cycles. Cylindrical form barely holds and brakes down after the slightest touch. Oxide film is totally removed alongside with other surface pollutants. Compare with Ni3 fuel in figure J7.